12-1995

Effects of Neutron Radiation on Resonant Cavity Light-Emitting Diodes

Daniel S. Hinkel

Effects of Neutron Radiation on Resonant Cavity

Light-Emitting Diodes

THESIS

Daniel S. Hinkel, Second Lieutenant, USAF

AFIT/GEO/ENP/95D-01

19960118 033

DTIC QUALITY INSPECTED 3

Approved for public release; distribution unlimited

AFIT/GEO/ENP/95D-01

Effects of Neutron Radiation on Resonant Cavity Light-Emitting Diodes

THESIS

Presented to the Faculty of the School of Engineering

of the Air Force Institute of Technology

Air University

In Partial Fulfillment of the

Requirements for the Degree of

Master of Science in Electrical Engineering

Daniel S. Hinkel

Second Lieutenant, USAF

December 1995

Effects of Neutron Radiation on Resonant Cavity Light-Emitting Diodes

Daniel S. Hinkel, B.S.E.E.
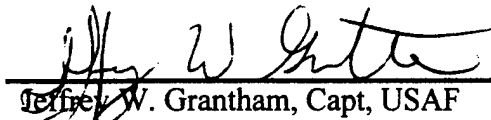Second Lieutenant, USAF

Approved:

Paul H. Ostdiek, Lt Col, USAF
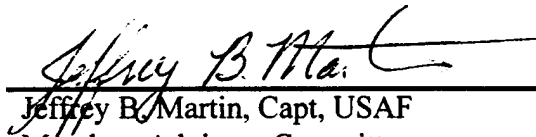Chairman, Advisory Committee

16 Nov 95

James A. Lott, Maj, USAF
Member, Advisory Committee

16 NOV 95

Jeffrey W. Grantham, Capt, USAF
Member, Advisory Committee

16 Nov 95

Jeffrey B. Martin, Capt, USAF
Member, Advisory Committee

22 Nov 95

Charles P. Brothers, Jr, Capt, USAF
Member, Advisory Committee

5 Dec 95

Preface

This thesis investigates the radiation hardness of Resonant Cavity Light-Emitting Diodes (RCLEDs). The study is motivated by the increasing application of RCLEDs to optical communication systems. An assessment of RCLED performance in radiation filled environment is a prerequisite for their use in future military systems.

This research project succeeded only because of the help of Lieutenant Colonel Paul Ostdiek, Major James Lott, Captain Jeff Grantham, Captain Mark Suriano, Major Greg Vansuch, and Mr Rick Patton.

My advisor, Lieutenant Colonel Paul Ostdiek, provided weekly motivation for this research project. He made numerous phone calls and inquires to various people on problems and concerns dealing with my thesis. When results were not working out he provided additional directions for the thesis. Without his help, this project would not have been possible. Major James Lott provided the initial motivation for the research. My thanks to Captain Jeff Grantham for providing the lab facilities to do the research. Thanks goes to Captain Mark Suriano who provided daily exchange of ideas and problem solving. Mark got me up to speed on radiation effects and facilitated contacts at Ohio State University. Many thanks to Major Greg Vansuch whose expertise in the laboratory and thorough knowledge of RCLEDs were essential to solving many of the problems along the way. He also spent many hours tutoring me on the lab equipment. Mr Rick Patton assembled fixtures for my thesis experimental setups. Without these fabricated devices the research would have been greatly hindered.

Thanks to Ohio State University (OSU) in cooperation with the Department of Energy (DOE) Reactor Sharing Program. Ohio State University provided the facilities to radiate the RCLEDs. This research would have been impossible with out their aid.

Thanks to Professor Kevin Malloy, University of New Mexico (UNM) Center for High Technology Materials (CHTM) for providing the devices (RCLEDs) for this project. Thanks also to Captain Brothers, USAF Phillips Laboratory for sponsoring this entire project.

Finally I would like to thank God for always being there when the going got rough (most of the time) and even when the going was not so rough. I would also like to thank my Mother Betsy and my Dad Steve for providing weekly support (over the phone); thanks mom---thanks dad. I would also like to thank my Sister Lisa for her support and inquiries about "radiating those what-ch-ma-call-it light bulbs things".

Dan Hinkel

Table of Contents

List of Figures

List of Tables

Table   **Page**

Abstract

Resonant Cavity Light-Emitting Diodes (RCLEDs) were irradiated in Ohio State University's nuclear reactor to determine the effects of Neutron displacement damage. The RCLEDs were characterized both before and after irradiation by their current versus voltage curves (I-V curves) and external light power versus current curves (L-I curves). The I-V curves showed an increase in the "knee voltage" at a neutron fluence of 1.45×10^{17} neutrons/cm^2. Logarithmic decreases in external light power and differential quantum efficiency were observed. Significant decreases in external light power were observed at neutron fluences greater than 5.1×10^{13} neutrons/cm^2. Equations were developed to predict the changes in external light power at a given bias current and the differential quantum efficiency for neutron fluences between 1×10^{10} neutrons/cm^2 to 1×10^{18} neutrons/cm^2. The damage constants for these equations were derived from the irradiation data. Finally, there was no significant changes in the RCLED output spectral distribution at neutron fluences up to 3×10^{15} neutrons/cm^2.

Effects of Neutron Radiation on Resonant Cavity Light-Emitting Diodes

1. Introduction

1.1 Problem Statement.

This thesis investigates the radiation hardness of Resonant Cavity Light-Emitting Diodes (RCLEDs). This encompasses characterizing RCLEDs both before and after irradiation by their bias current versus voltage curves (I-V curves) and external light power versus bias current curves (L-I curves). Equations are developed to predict the changes in external light power at a given bias current and the differential quantum efficiency for neutron fluences between $1x10^{11}$ neutrons/cm^2 to $5x10^{17}$ neutrons/cm^2. The damage constants for these equations are also determined from the irradiation data. Finally, the spectral distribution of the outputs of the RCLEDs is analyzed at neutron fluences up to $5x10^{15}$ neutrons/cm^2.

This research is motivated by the need for radiation hard, low cost sources for fiber optic communication systems, as well as arrays of sources for optical computing. The radiation hardness of the RCLEDs is critical if these devices are to be used in a radiation filled environment such as space. Further motivation is presented in Section 1.2. Also presented is the device structure of a RCLED and its operation. Electro-luminescence, and radiation hardness are outlined since these are the areas of concern for this research project.

1.2 Background

Historically, the most popular means of generating light came from incandescent lamps. Unfortunately, these broadband white light sources are not well-suited for optical interconnects or fiber optic communication. Fiber optic communications require a high intensity, narrow bandwidth light source. The optical interconnects, which allow fiber optic cable to be used in long distance communication, are driven by one of two methods. One optical interconnect is the Modulator-Receiver link. Unfortunately, this method has the inherent problem of requiring a bulky power supply where space is considered 'prime real-estate' so an alternative method was devised. This alternative method is the Emitter-Receiver link and this encompasses using an on-chip diode laser. Unfortunately, the laser requires extra power to overcome the threshold conditions to achieve lasing. A desirable replacement for both the Modulator-Receiver link and the Emitter Receiver link would be a photonic device that has the property of taking up a small amount of real-estate and also being a thresholdless device.

In the 1960's a new photonic device, the light emitting diode (LED), was demonstrated. This device was a possible solution to the optical interconnect problem [1]. In the LED's infancy it was not able to compete in intensity with the on-chip lasers or even incandescent lights and therefore had the task of low definition displays and very short distance communications. However, in the late 1980's, with the emergence of new high-brightness LEDs, these devices became a viable alternative to incandescent lamps in applications such as the tail lights of automobiles and street lights. These new LEDs save automobile consumers millions of dollars in replacement costs because, conceivably, the LEDs last longer, up to a million hours or more (longer than the lifetime of the

2

automobile) [1]. However, these new LEDs could not compete with the laser in applications such as high-definition displays and long distance communication.

Finally in the early 1990's, the idea of 'mating' the LED and the laser's cavity came about. The LEDs were transformed into the vertical cavity or resonant cavity-light emitting diode (RCLEDs). This photonic device combined the desirable properties of both devices: the LED's, low cost and long life with the laser's high intensity, narrow line width, short coherence time, and narrow divergence [2]. These properties suggest that RCLEDs are suitable for the task of optical interconnects.

The 'heart' of the RCLED is the Fabry-Perot cavity. The Fabry-Perot cavity ensures that the field distribution reproduces itself in relative shape and phase after a round trip through the system. In other words, certain characteristic modes are favored and therefore maintained. The Fabry-Perot enhances intracavity fields and serves as a narrow band spectral filter. If we couple this phenomenon with the addition of strategically placed, band gap engineered quantum wells, a designable peak emission wavelength is achieved [3].

Both RCLEDs and LEDs generate photons in the same fashion. A bias is placed across the p-n junction which enhances the radiative recombination of the injected electrons and holes. These photons are constrained to certain modes by the Fabry-Perot cavity. A specific mode is selected by matching these allowed cavity modes with the quantum well's discrete energy levels.

1.2.1 Device Structure.

RCLEDs are made up of three main components: 1) Distributed Bragg Reflectors (DBRs), 2) Fabry-Perot Cavities (FPCs), and 3) a Quantum Well (QW) active region.

3

They are a type of semiconductor photonic device with the cavity oriented normal to the

planes of material growth. A general overview of each of these follows.

1.2.1.1 Distributed Bragg Reflectors.

The Distributed Bragg Reflectors which are used as the mirrors of the RCLED's Fabry-

Perot cavity are formed by growing alternating semiconductor epitaxial layers of lattice

matched materials. The differing refractive indexes of the alternate layers enhances the

overall reflection coefficient (the greater the difference the higher the reflectance). The

alternating layers are each a quarter wavelength thick, and reflectance increases with the

number of layers [4]. According to Verdeyen, "These mirrors do not represent new

technology, just a new and innovative application for an old theory from transmission

lines [5]." An example of a mirror is shown below in Figure 1. The RCLED's Fabry-

Perot cavity is bounded by two of these DBR mirror structures.
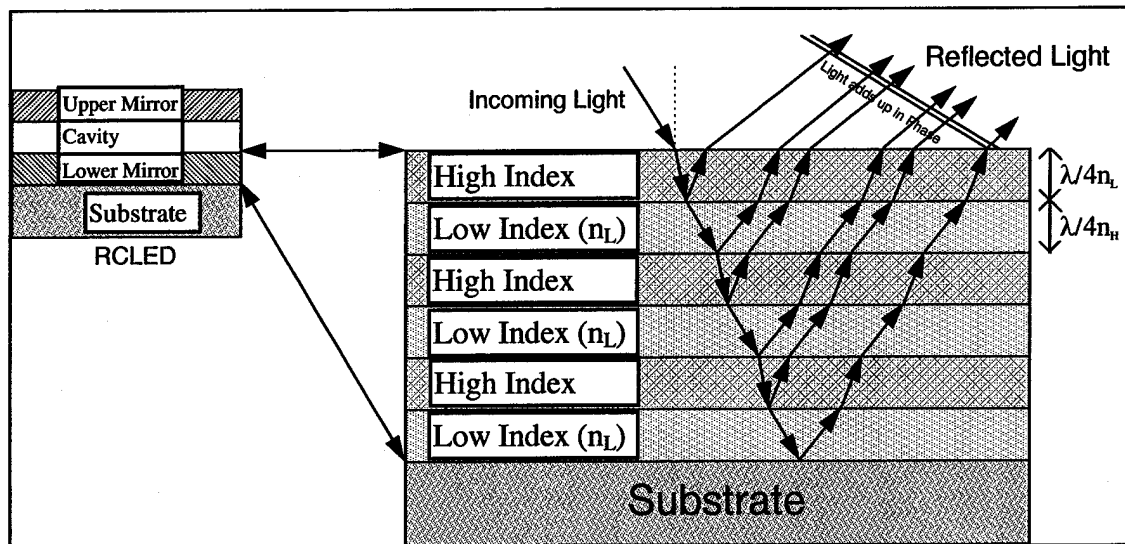
Figure 1. Expanded view of a RCLED mirror or Distributed Bragg Reflector [2].
It is composed of alternating layers of high/low refractive index material.
Incoming light is reflected back in stages and adds up in phase as shown above.
Each layer is a quarter wavelength in thickness.

1.2.1.2 Fabry-Perot Cavity.

The Fabry-Perot cavity, shown in Figure 2, ensures the field distribution reproduces itself in relative shape and phase after one round trip through the system, thereby maintaining that mode. The Fabry-Perot cavity is governed by the simple relation: $d=q\lambda/2n$, where d is the distance between the two 'highly' parallel mirrors of the Fabry-Perot cavity, q is an integer, and λ is the design wavelength. The mirrors of the Fabry-Perot cavity are distributed Bragg reflectors composed of alternating layers of high/low refractive index layers. When each of these layers have an optical thickness equal to one quarter of the design wavelength they act as the Fabry-Perot cavity mirror [4]. For resonance to occur, there has to be an integral number of half wavelengths between the two mirrors. Because of the desired dimensions, this means that the integer q is a very large number for optical frequencies. For example, if the refractive index of GaAs is 3.6 and the cavity length d is 100μm, the q value is approximately 900 [5].

The Fabry-Perot cavity acts as a pass band for the generated photons. This pass band is called the Fabry-Perot dip and controls the emitted spectrum in wavelength (and its FWHM).
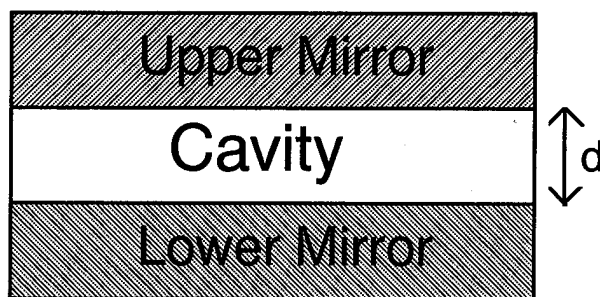
Figure 2. Basic Fabry-Perot Cavity [2]

The RCLED design goal is to match one of these Fabry-Perot cavity modes with quantum wells used to generate the photons.

1.2.1.3 Quantum Wells.

Quantum wells (QWs) are used in devices because they are efficient at generating photons. QWs allow the design of the peak emission wavelength. To couple efficiently with the cavity, the quantum wells are placed at the peak of the standing wave of the electric field associated with the Fabry-Perot modes. The wavelength of the peak emission from the quantum well must match the Fabry-Perot cavity mode where $\lambda=2nd/q$ as stated above. Figure 3 shows a typical QW with its allowed discrete energy levels.
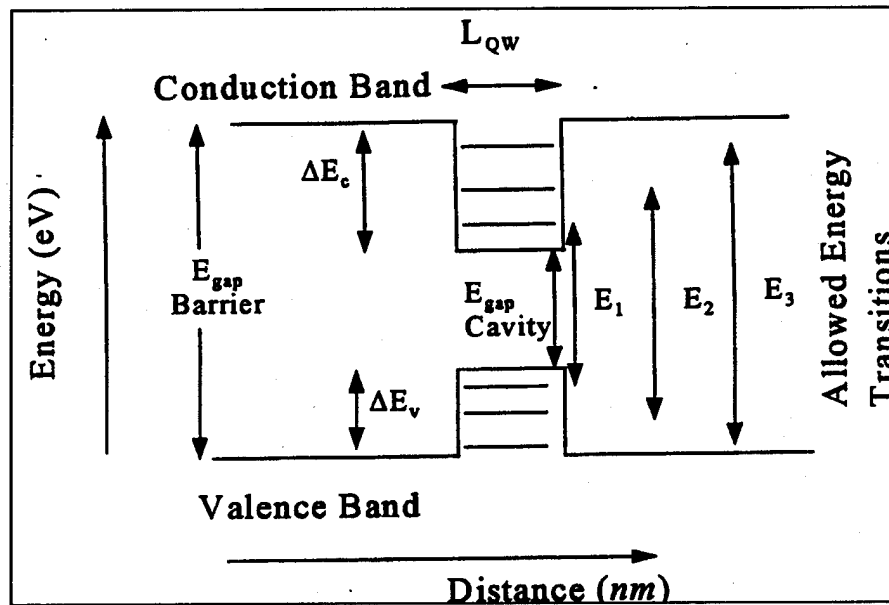
Figure 3. Quantum Well showing discrete energy levels. L_{QW} is the width of the well. ΔE_c is the conduction band offset and ΔE_v is the valence band offset [2].

1.2.2 Theory of Operation of RCLED Structure.

Combining the ideas of the distributed Bragg reflector, Fabry-Perot cavity, and quantum wells into one structure yields a RCLED. Their combined structure and

characteristics take what was once a low intensity, broadband photonic device (a LED) and turns it into an enhanced microcavity photonic device that yields a high intensity and narrow line width output. A composite diagram of the RCLED is shown in Figure 4.
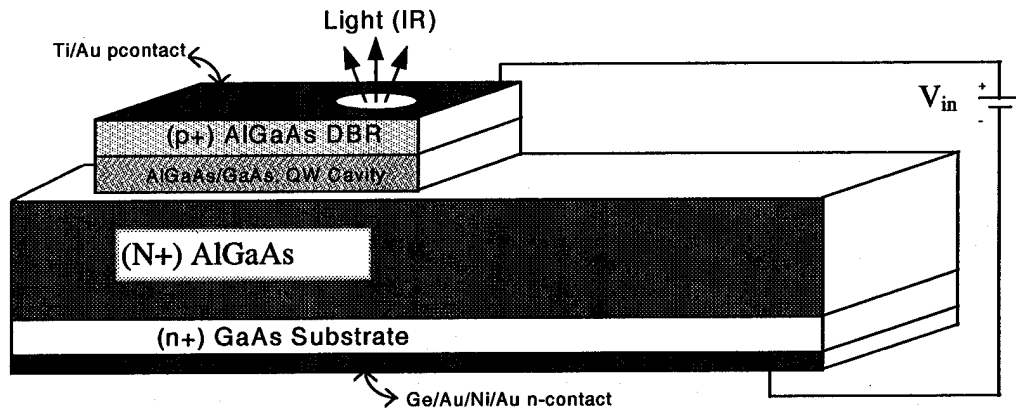
Figure 4. Composite RCLED structure. The DBRs (mirrors) are made from AlGaAs and the upper contact is made of Gold. This device emits light in the infrared region [2].

Infrared emitting RCLEDs are made from the III-V compounds, based on Gallium Arsenide (GaAs), with bandgaps that allow emission of infrared light between 800 nm and 900 nm. A comparison of a RCLED with a conventional LED (see Figure 5) shows a considerably narrower full width at half max (FWHM) for the RCLED.

The decreased FWHM is due to the Fabry-Perot Dip in the reflectivity spectrum. The reflectivity of this Fabry-Perot Cavity decreases around 840 nm. This decrease in reflectivity also depends on the angle, from the normal, that the light is emitted. These dependencies allow the RCLED shown in Figure 6, to emit or transmit in the 840 nm to 850 nm wavelength region.
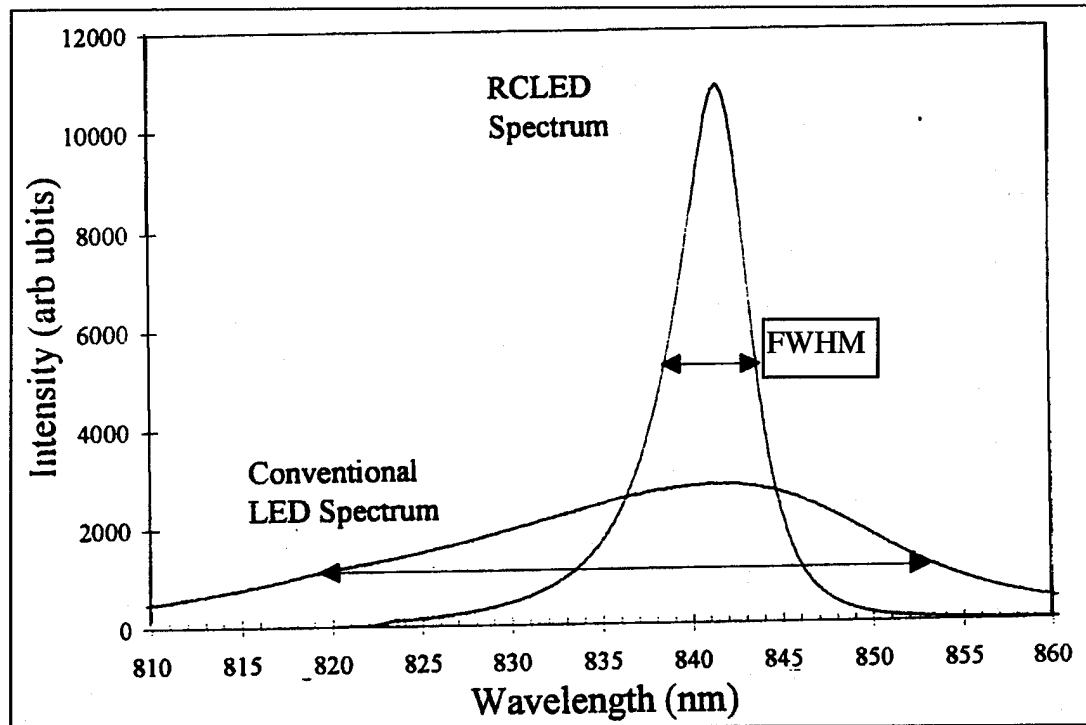
Figure 5. Comparison of a conventional LED's Spectrum with that of a RCLEDs [2].
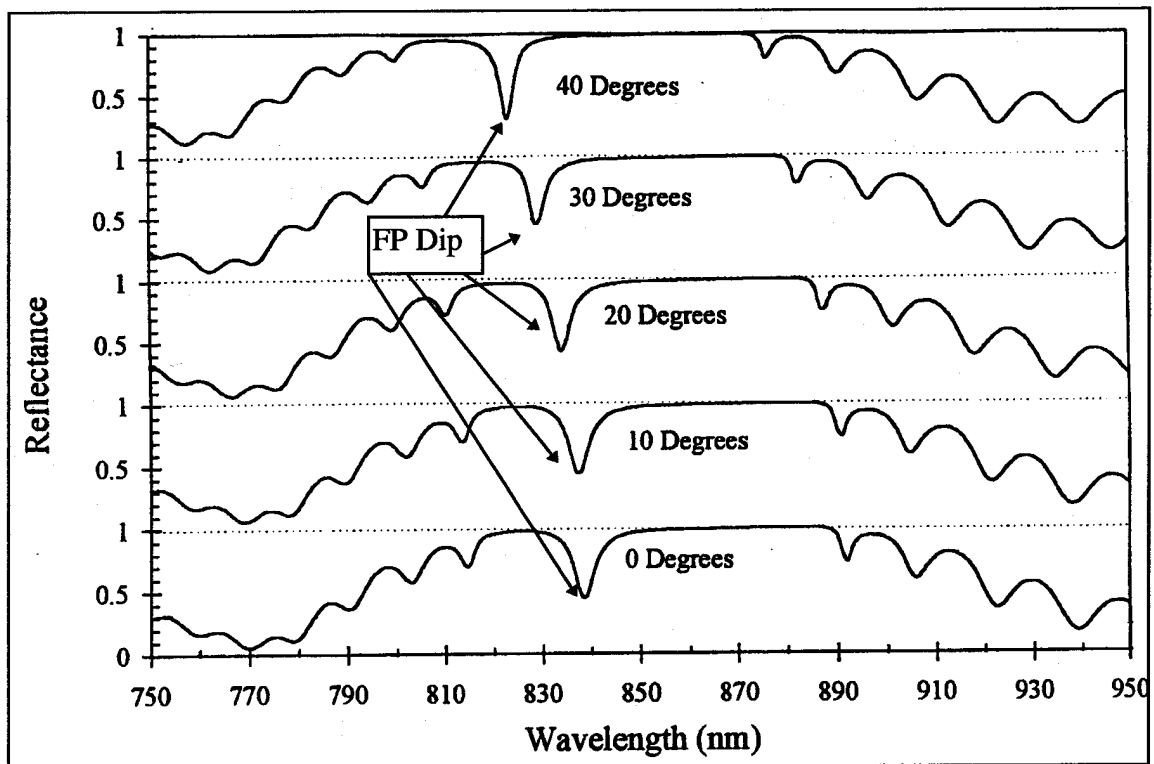
Figure 6. Reflectance spectrum of a typical RCLED (this is not the RCLEDs used in this research project). Zero degrees represents normal incidence.

Related to the RCLEDs reflectance is its transmittance. The transmittance is one minus the reflectivity (ignoring absorption). Figure 7 shows the transmittance of a RCLED and depicts the sensitivity of the FWHM on the transmittance (or 1-reflectivity) of the mirrors forming the Fabry-Perot Cavity.

The Free Spectral Range (FSR) is also shown in Figure 7, which is simply the longitudinal mode spacing, governed by FSR=c/2nd. Here c is the speed of light, n is the effective index of refraction of the spacer, and d is the effective distance between the mirrors. Notice how the FWHM decreases as the reflectivity of the mirrors used to form the cavity is increased.
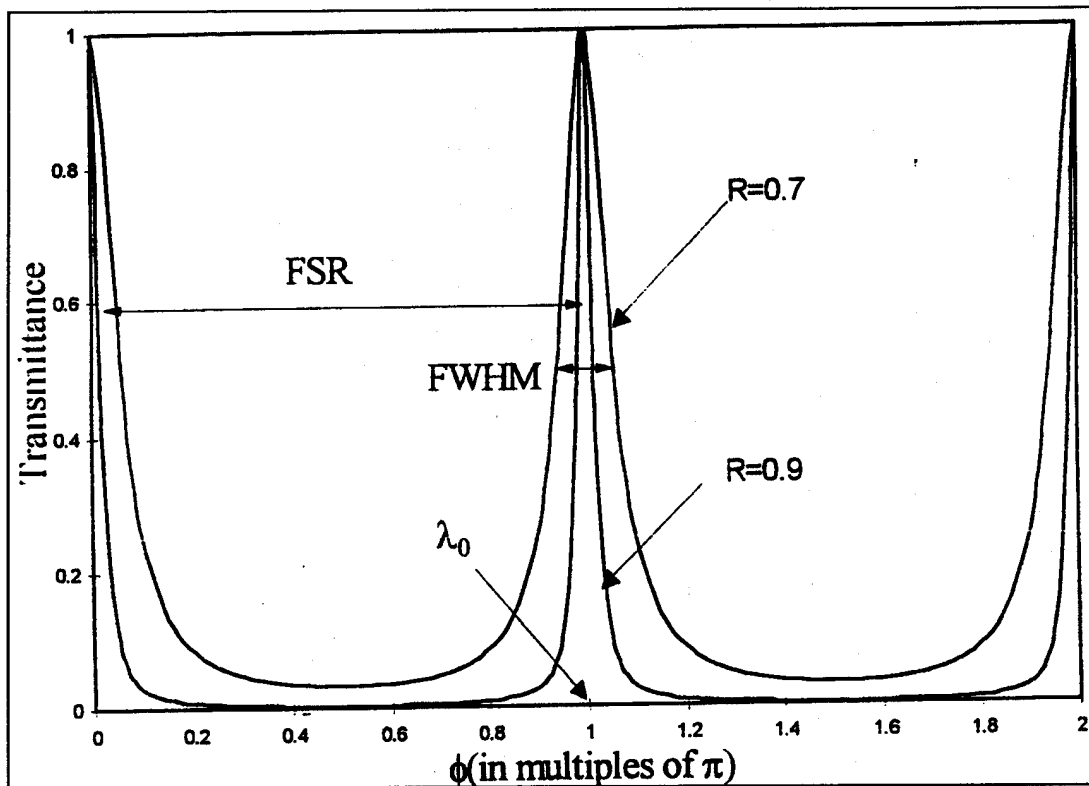
Figure 7. Transmittance of a RCLED, showing the FWHM for different reflectivity's of the Fabry-Perot Cavity. The Free Spectral Range is also shown [2].

For fiber optic communication then, a RCLED is preferred over a conventional LED because of its narrower spectrum. This preferred characteristic results from the Fabry-Perot Cavity selecting out the pass band of transmission, or transmission peak (the reflectivity dip between 830 to 850 nm). A conventional LED can not compete with the performance of the RCLED because it does not use QWs for more efficient photon generation and does not utilize a Fabry-Perot cavity with its spectral pass band characteristics.

For more details on RCLEDs, see Fitzgerald (AFIT, Thesis), 1994 [2]. Now that a basic understanding of what RCLEDs are and how they work is in hand, the main topic of radiation hardness of RCLEDs, can be discussed.

1.2.3 Radiation Hardness

The radiation hardness of RCLEDs is the main interest of this thesis, which is basically an investigation of the behavior of Resonant Cavity Light-Emitting Diodes under the influence of damaging incident radiation. The damaging incident radiation comes from neutrons that mainly cause atomic displacement damage in semiconductor materials; in this case GaAs and AlGaAs. This displacement damage results from atoms being displaced from their lattice site. Small displacement damage are point defects or Frenkel defects which are interstitial-vacancy pairs. On the other hand, large displacement damages are large regions of vacancies created from an avalanche of displaced atoms (a cascading effect).

To determine the effects of the damage created by the radiation, the RCLEDs are characterized spectrally by the peak wavelength and full-width-half-max, current-voltage curves, and luminous power-current curves prior to radiation. Then they are re-

characterized after being irradiated. This was accomplished for at least ten different neutron fluences. A neutron fluence meaning the number of neutrons passing through an area. A damage constant, K, is determined from the slope of a line fitting the plotted data points versus the neutron fluence (Φ). A simple form of the equation is:

$$y = k\Phi + b \tag{1}$$

where the variable y represent any parameter desired, i.e., light power (from L-I curves), "knee voltage" (from I-V curves), and slope efficiencies all versus neutron fluence Φ.

The degradation of the RCLEDs characteristics (L-I, I-V, quantum efficiencies, etc..) can be linked to the reduced lifetime of the minority carriers near the p-n junction. The probability, of minority carriers combining with majority carriers and generating photons, is reduced. If fewer radiative recombinations occur, then the efficiency of the device decreases. This means that more electron-hole pairs are being used in nonradiative processes (no photons generated) than in radiative processes (photons generated). This idea and these terms are explained in section 2.1.

The work done in this thesis considers only the effects caused by the total neutron fluence. This is a general overview of what radiation damage is and how to determine its effects. The scope of the research project will be discussed next.

1.3 Scope.

The scope of this thesis is to determine the effects of displacement damage caused by neutron radiation on infrared $Al_xGa_{1-x}As$ RCLEDs (emitting in the 844 nm range). This research project was intended to be an experimental thesis that supporting on going theoretical work. The research was accomplished in two main steps. First, the RCLEDs

(designated E231) were characterized before and after irradiation. Then an equation was fit to the data points so that future predictions of the RCLED's characteristics are possible.

A proper annealing study was not performed because the needed resources were not available. The reactor's beam port did not allow measurements of electrical or optical properties of the sample. These properties would be needed for a proper annealing study. Measurements would also be needed as soon as the samples were pulled from the reactor but this would compromise radiation safety procedures. However, a cursory annealing study was accomplished in an attempt to discover if short-term annealing affected the results.

1.4 Method of Presentation

The theory on radiation effects is presented in Chapter II. The experimental setup is described in Chapter III. Experimental results and comparison to theory is located in Chapter IV and finally in Chapter V, the conclusions and recommendations are presented.

II. Theory

2.1 Basic Defining Characteristic of LEDs

For the purposes of this thesis, there are four parameters that are used to characterize the RCLEDs: 1) external quantum efficiency, 2) responsivity, 3) the overall quantum efficiency (wall plug efficiency), and 4) spectral emission width. The external quantum efficiency is defined as the slope of the output light power (L_{tot}) versus bias current (I_{Bias}) times its corresponding junction voltage (V_j) [3].

$$\eta_{ex} = \frac{\Delta L_{Tot}}{V_j \Delta I_{Bias}} \quad \text{(unitless)} \tag{2}$$

η_{ex} also equals:

$$\eta_{ex} = \eta_e \eta_i \quad \text{(unitless)} \tag{3}$$

where η_e is the overall transmission efficiency and η_i relates the internal photon flux to the injected electron flux. Photon flux is the number of photons passing through an area in a finite time period.

The responsivity (R) is defined by [3]:

$$R = \eta_{ex} \frac{1.24}{\lambda_o} \quad \text{(watts/amp)} \tag{4}$$

The responsivity is simply the emitted light output power divided by the injected bias current.

$$R = \frac{P_{out}}{i} \quad \text{(watts/amp)} \tag{5}$$

Finally the overall quantum efficiency η (wall plug efficiency) is:

$$\eta = \frac{P_o}{iV} \qquad \text{(unitless)} \qquad (6)$$

where P_o is the emitted optical power and V is the voltage drop across the device. For the

purposes of this thesis the wall plug efficiency is going to be approximated as equal to the

external quantum efficiency. The external quantum efficiency uses the voltage across the

junction, while the wall plug efficiency uses the voltage across the device. It is assumed

that when a bias current is sent through the RCLED, the junction voltage and the

measured voltage across the device are approximately equal (i.e., the series resistance R_s

is small see Figure 8).
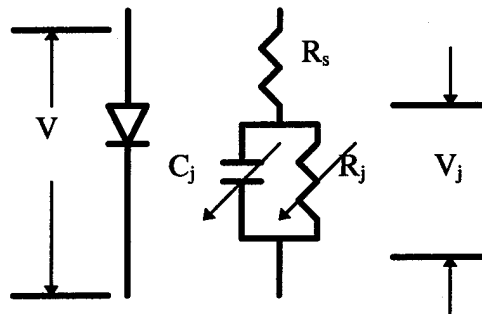
Figure 8. Diagram showing the series resistance (R_s), junction resistance
(R_j), junction voltage (V_j), junction capacitance (C_j), and the voltage
across the entire diode (V).

These are some of the standard parameters used to characterize LEDs. The

external quantum efficiency, responsivity, and the overall quantum efficiency (wall plug

efficiency) will be calculated before and after the RCLEDs are irradiated. The

calculations for pre-irradiation will lend some understanding of how RCLEDs relate to

normal LEDs, and post-irradiation calculations will add to the radiation study of this

thesis.

14

2.2 Radiation Effects

Incident neutrons generate defects in the semiconductor lattice atoms. These defects are caused by reactions or interactions of neutrons with lattice atoms (scattering). In scattering reactions, the neutron remains free at a reduced energy. It has less energy because some of its kinetic energy has been transferred to the lattice atoms with which it collides. If the scattered atom is unable to find a vacant location in the lattice, then the generation of interstitials and vacancies occurs. Interstitials are atoms resting in nonequilibrium positions in the lattice, where as vacancies are empty equilibrium sites. If there are enough of theses vacancies and interstitials created, permanent changes in the physical properties of the material may result. These vacancies and interstitials are defects in the lattice, which introduce energy states in the band gap. These defect energy states may serve as efficient recombination and trapping centers, which enhance minority carrier recombination and thus reduce the minority carrier lifetime.

The two major types of defects can be classified as vacancy-interstitial pairs (point defects) and defect clusters. Defect clusters come about by a recoil or avalanche effect (cascading effect). The recoil effect begins when a neutron scatters an atom. The recoil atom then leaves a vacancy, and if it has enough energy, collides with another lattice atom. The process continues until all of the recoil atoms come to rest. Possible effects from all of these defects include changes in electrical properties such as carrier lifetime, electrical resistance, and carrier mobility. These will in turn affect the external quantum efficiency, the bias current versus voltage curves, and the light output power versus bias current curves.

The general minority-carrier-lifetime equation from Messanger and Ash [7] relates the neutron fluence to the lifetime of the carriers:

$$\frac{1}{\tau} = \frac{1}{\tau_o} + \frac{\Phi}{K} \qquad (\text{sec}^{-1}) \qquad (7)$$

Where τ is the lifetime of the carriers, τ_o is the pre-irradiated lifetime, K is a damage constant, and Φ is the neutron fluence in neutrons/cm^2. According to Walsh [8] the internal quantum efficiency is proportional to τ which is proportional to the differential quantum efficiency, $\Delta\eta$. Knowing this, the differential quantum efficiency is related to the neutron fluence by:

$$\frac{1}{\eta(\Phi)} = \frac{1}{\eta_o} + \frac{\Phi}{K_\eta} \qquad (\text{unitless}) \qquad (8)$$

Where $\eta(\Phi)$ is the differential quantum efficiency after irradiation, η_o is the pre-irradiation value of differential quantum efficiency, Φ is the neutron fluence, and K_η is the damage constant (neutrons/cm^2) to be determined. It is evident that the $\eta(\Phi)$ is inversely proportional to the neutron fluence and dependent on the damage constant. Equation (8) can be rewritten in the form of:

$$\eta(\Phi) = \left(\frac{1}{\eta_o} + \frac{\Phi}{K_\eta} \right)^{-1} \qquad (\text{unitless}) \qquad (9)$$

This is the form of the equation that will be utilized to model the response of differential quantum efficiency to different neutron fluences.

16

A similar form of equation (9) can be found for the total light power L_{tot}, at a given bias current, versus neutron fluence.

$$L_{tot}(\Phi) = \left(\frac{1}{L_{tot}} + \frac{\Phi}{K_{L_{tot}}} \right)^{-1} \qquad (\mu W) \qquad (10)$$

Where $K_{L_{tot}}$ (μW x neutrons/cm^2) is the damage constant to be determined from the experimental data, and L_{tot} is the pre-irradiation value of the total light power emitted from the RCLED. Again $L_{tot}(\Phi)$ is inversely proportional to the neutron fluence (Φ) and dependent on $K_{L_{tot}}$.

It is important to determine if the RCLED's performance can be improved after irradiation because annealing may reduce the damage. Annealing of radiation damage refers to the partial or total self-healing of a device after exposure. The term healing refers to the disappearance of the defects due to vacancy-interstitial recombination. The two forms of annealing that are dealt with in this thesis are isochronal and isothermal annealing. Isothermal is waiting a certain time period (at constant temperature) so that effects of the damage are reduced. Isochronal is accomplished by increasing the temperature (at constant time) which increases the internal thermal energy. By increasing the thermal energy, the random movement of atoms is increased. This increases the chances of filling vacant lattice sites thereby decreasing the annealing time. This is the basic theory used in the analysis section to compare with the experimental results.

III Experimental Approach and Setup

3.1 Experimental Approach.

The Resonant Cavity Light-Emitting Diodes (designated E231) were characterized both before and after irradiation by the bias current versus voltage curves (I_{bias}-$V_{measured}$), light power versus bias current ($L_{measured}$-I_{bias}) curves, and spectrally by the peak wavelength λ_{peak} and full width at half maximum (FWHM) of the emitted light.

These data were converted into parameters such as differential quantum efficiency ($\Delta\eta$) versus neutron fluence (Φ), and total light power emitted by the RCLED (L_{tot}) versus neutron Fluence (Φ). With this data, an equation was fit to the data points, and a damage constant K was determined. This K allows prediction of $\Delta\eta$ and L_{tot} versus neutron fluence.

The final experimental data collected dealt with the effects of annealing. First, the RCLEDs were isothermally annealed. In this case, three sample sets of RCLEDs were characterized, then set aside for a week and recharacterized (all this taking place at room temperature). Second, isochronal annealing was performed. In this case, the temperature of the same three sample sets of RCLEDs were raised to speed up the time factor. This was accomplished by placing the RCLEDs directly on a hot plate. The temperature of the hot plate was measured using a thermal couple. The RCLEDs were characterized both before and after being heated.

3.2 Electro-Luminescence Experimental Setup.

Electro-luminescence (EL) is accomplished by placing a current through a

RCLED. Carriers are injected and eventually recombine with holes in the quantum wells

and photons are emitted. The emitted wavelength is determined from the Fabry-Perot

Cavity which selects the pass band of transmission, with a typical emission peak at 844

nm (for the RCLEDs E231). The EL experimental setup is shown in Figure 9.
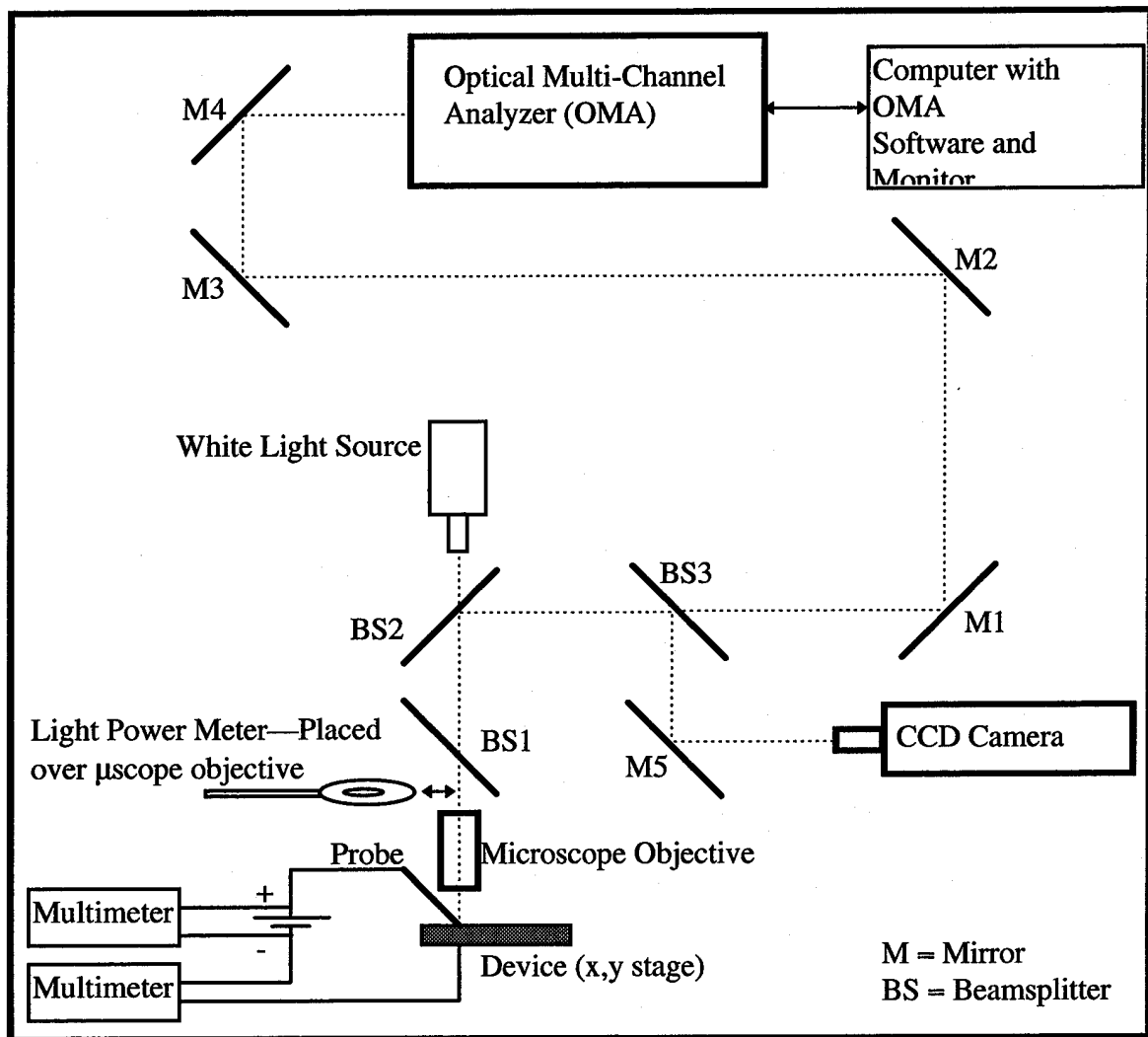
Figure 9. General experimental setup for Electro-luminescence [2]. Where beam
splitters are represented by BS, and mirrors are represented by M.

Shown in Figure 10, Figure 11, and Figure 12 are photographs of the lab equipment. They represent three different views of the same setup. They also show the various equipment used to take the measurements.
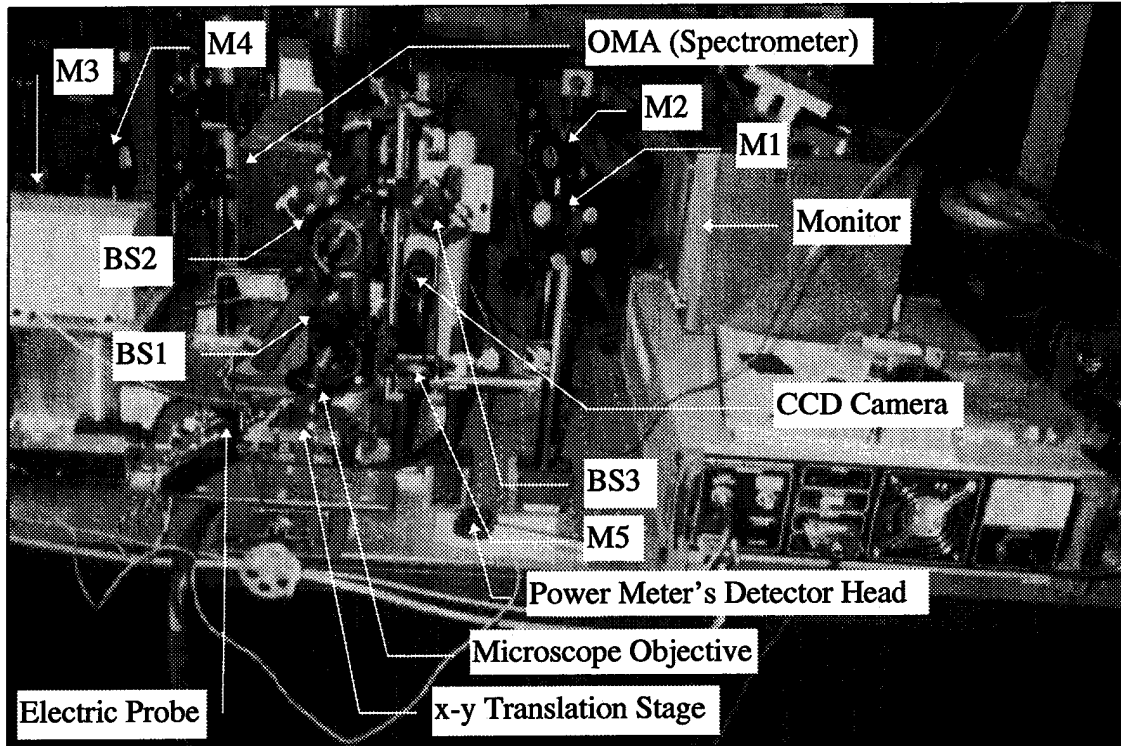
Figure 10. Electro-Luminescence setup showing the translation stages, the beam splitters, mirrors, microscope objective, CCD camera, and its corresponding monitor. The side of the optical multi-channel analyzer (OMA) is also shown.

The RCLED sits on the x-y translation stage and then the electric probe is placed on top of a test RCLED. The test RCLED is found by using the CCD (charge couple device) camera and monitor. They enable the user to place the electric probe on any RCLED desired. The light path goes from the RCLED through the microscope objective (collimating the light), passes through BS1, reflects off of BS2 and BS3, and finally reflects off of M5 into the CCD camera (refer to Figure 9 for the block diagram). The

CCD camera sends the image to the monitor so the user has a real time display for aligning the RCLEDs.

To get the light into the OMA (optical multi-channel analyzer), the light path goes from the RCLED through the microscope objective, passes through BS1, reflects off of BS2, passes through BS3, and then reflects off of M1, M2, M3, M4, and into the OMA.

In the lower left center of the Figure 10, laying on a white index card, is the power meter's detector head.

Shown in Figure 11 is a close-up view of a portion of Figure 10. This shows the ground plane that the RCLEDs rest on, the electrical pumping probe, and the microscope objective that collects the emitted light from the RCLEDs. Also shown is the x-y translation stage that enables very fine movements of the RCLEDs for alignment purposes. Not shown is the power meter's detector head. When making measurements, the detector head swings in over top of the microscope objective.
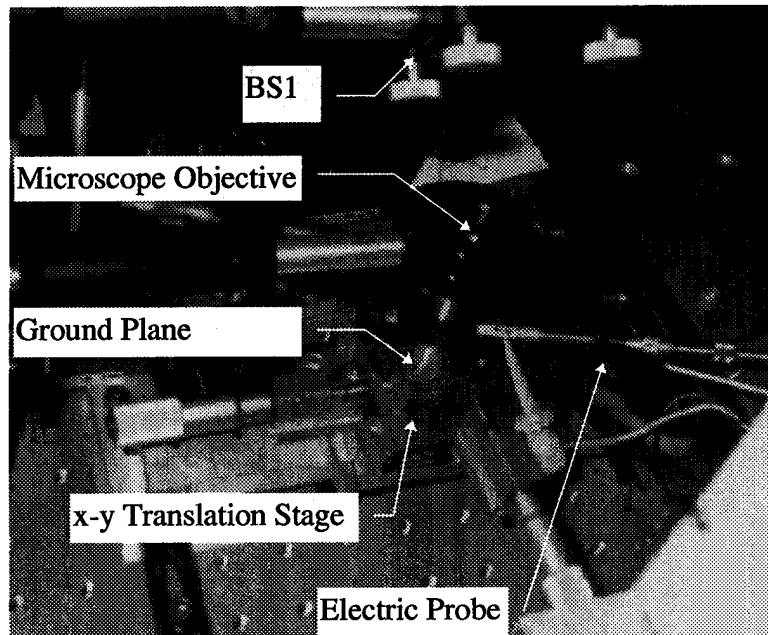
Figure 11. Expanded view of Electro-Luminescence setup.

In Figure 12 is another view of the electro-luminescence setup. It shows the OMA on the left and the multimeter used to measure the voltage in the center, and the power meter used to measure the emitted light power in the center-front of the figure. Not shown is another multimeter used to verify the amount of current biasing the RCLEDs.
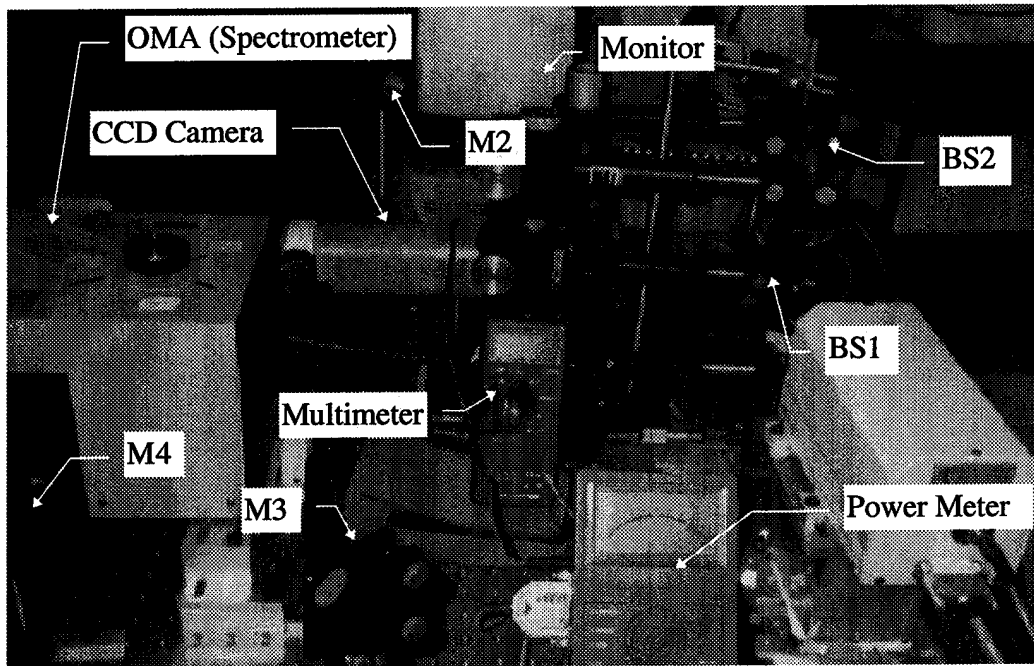
Figure 12. Another view of the Electro-Luminescence Setup.

3.3 Resources

All measurement resources are located in Bldg. 194 on area B of WPAFB (AFIT Photonics Lab). For the Electro-luminescence measurements, all of the equipment utilized is shown in Table 1.

Table 1. Equipment Listing for Electro-Luminescence

Optical Multichannel Analyzer (OMA)	Manufacture	Princeton Applied Research
	Model	EG&G 1460
	Accuracy	+/- 3Å
CCD (charged coupled device) camera	Manufacture	COHU
	Model	Solid State Color Camera
Diode Focusing Lens	Manufacture	Melles Griot
	Focal Length	2.54 cm
	Spot Size	1.85 μm
Electric Probe Precission Manipulator	Manufacture	Micromanipulator Company
	Model	110
Precision Pulsed Current Source	Manufacture	ILX Light Wave
	Model	LDP-3811
Multimeters	Manufacture	Fluke
	Model	77/AN
x-y Translation Stage that is electrically grounded	Manufacture	AFIT Grad Student
	Model	Rigged
IR Dielectric Mirrors	Manufacture	New Focus
	Model	5102-NIR
Power Meter	Manufacture	Coherent
	Model	Field Master

The RCLEDs used in this thesis are designated E231 and were grown by University of New Mexico Center for High Technology Materials. Their characteristics are given in Table 2. The RCLED's mirror layers are linearly graded to reduce their electrical resistance. The resistance is due to abrupt conduction and valence band energy offsets at hetero-junctions that act as barriers to current flow. By grading the interface, the junctions are less abrupt and resistance to current flow is decreased [2].

Another resource was Ohio State University's nuclear reactor used to irradiate the RCLED samples. They were able to irradiate the RCLEDs at all neutron fluence desired for this work. The test matrix used is located in Table 3.

Table 2. Epitaxial Structure of RCLED E231

	RCLED E231
Ohmic Contact	200 Å GaAs Ca p+doped (C)
Upper DBR (HL)	$Al_{0.15}Ga_{0.85}As$/AlAs (linearly graded) p-doped (C)---6HL
Cavity	1λ $Al_{0.15}Ga_{0.85}As$/AlAs (linearly graded over 998 Å)
Quantum Wells	Four 8nm GaAs QWs with 10nm $Al_{0.15}Ga_{0.85}As$ Barriers
Lower DBR (HL)	$Al_{0.15}Ga_{0.85}As$/AlAs (linearly graded) n-doped (Si)---38.5HL
Substrate	GaAs n+ doped (Si)

Table 3. Test Matrix (Radiation Dates)

RCLED Sample	kW-min	(1 MeV Si) Φ (neutrons/cm^2)	Rad Date (1995)	# Days Resting	I-V	# Days Resting	L-I	Annealing Study (1995)
3	0.05	1.0E+11	25-Aug	12	9-Sep	19	14-Sep	------
6	0.5	1.0E+12	25-Aug	12	9-Sep	19	14-Sep	------
10	1	2.0E+12	8-Sep	6	14-Sep	6	14-Sep	------
5	5	1.05E+13	23-Aug	5	28-Aug	16	14-Sep	------
2	25	5.0E+13	23-Aug	7	30-Aug	14	14-Sep	20-Sep
7	25	5.0E+13	8-Sep	6	14-Sep	7	14-Sep	------
4 (crushed)	100	2.0E+14	25-Aug	-------	------	------	------	------
8	500	1.0E+15	11-Sep	3	14-Sep	3	14-Sep	20-Sep
9	1500	3.0E+15	8-Sep	6	14-Sep	6	14-Sep	20-Sep
1	72000	1.5E+17	22-July	22	14-Aug	52	14-Sep	------

Finally, this section examines the neutron fluences used in this study and are presented in Table 3 (taken from Suriano, 1995 [AFIT thesis]). All of the neutron flux monitoring was performed at Ohio State by the reactor staff. A neutron flux wire was placed in the same configuration as the samples in order to determine a neutron flux. A differential energy flux is calculated through the SAND-II neutron spectrum unfolding code. The spectrum is obtained from the activation of the multiple flux wires along with assumptions of the spectrum's shape between fission and thermal energies. The spectrum shapes are normally chosen to be Maxwellian for the thermal range (0~0.5 eV), 1/e for the resonance region (0.5 eV ~ 1.0 MeV), and a fission spectrum, $\chi(E)$, for the fast region

(1.0 MeV -∞) based on the reactor's fuel. This differential spectrum is used to calculate

the 1 MeV equivalent fluence in accordance with ASTM E 722-85. The flux

measurement is important since the damage constant is based on the exposure of the

samples. The spectrum drops sharply around 1 eV due to the cadmium cutoff. Cadmium

was used to cover the samples to reduce thermal neutrons thereby reducing the activation

products.

This finishes the Resource chapter. Measured data is presented in the

Experimental and Discussion chapter.

IV Experimental Results and Discussion

This chapter is divided into seven sections: 1) relative light intensity versus bias current for varying neutron fluences (Φ), 2) total output light power versus Φ, 3) differential quantum efficiency versus Φ, 4) responsivity versus bias current for varying Φ, 5) bias current versus voltage curves for a specific Φ, 6) how Φ effects the emitted spectral characteristics, and 7) isothermal and isochronal annealing effects. The plots are not data of single devices; they are averaged data for a set of five to ten similar devices. However, the individual curves are consistent with each averaged curve.

The performance of the RCLEDs is degraded by exposure to different neutron fluences. A typical result for the relative emitted light power of the 50 μm aperture RCLEDs, as a function of forward bias current at several different neutron fluence levels, is shown in Figure 13. There is a general trend of continued degradation of relative light power with higher neutron fluences. Notice the jump in degradation between curve #5 and #6 at 5×10^{13} neutrons/cm^2 and curve #7 at 3×10^{16} neutrons/cm^2.

Located on the Pre-irradiation (Prerad) and Sample #1 curves, are uncertainties in the measurements. The uncertainty bars represent the standard deviation from the mean of light power (for 5 to 10 devices) for a given current. The rest of the curves have similar uncertainties but were not plotted, for the purpose of a clearer figure. Devices represented by curves #5 and #6 were irradiated at the same neutron fluence of 5×10^{13} neutrons/cm^2. This shows that there is repeatability, i.e., similar results are expected for future RCLEDs (of the same compositional make up) at these neutron fluences.

Prerad Vs Postrad L-I Curves

Legend:
- —— Prerad 50 um Aperture
- Postrad Sample #5 50um Aperture
- Postrad Sample #4 50um Aperture
- Postrad Sample #6 50um Aperture (Repeatability with Sample #2)
- Postrad Sample #7 50um Aperture
- Postrad Sample #8 50um Aperture
- Postrad Sample #3 50um Aperture
- Postrad Sample #1 50um Aperture
- Postrad Sample #2 50um Aperture

****These L-I Curves for each Sample are averages of individual RCLED L-I Curves.

**NOTE–The individual L-I Curves match the average L-I curves in Line Shape.

#9 no emitted light

Neutron Fluence	Sample #
none	Prerad
1.0×10^{11} neuts/cm^2	1
1.0×10^{12} neuts/cm^2	2
2.0×10^{12} neuts/cm^2	3
1.0×10^{13} neuts/cm^2	4
5.0×10^{13} neuts/cm^2	5
5.0×10^{13} neuts/cm^2	6
1.0×10^{15} neuts/cm^2	7
3.0×10^{15} neuts/cm^2	8
1.5×10^{17} neuts/cm^2	9

X-axis: Bias Current (mA)
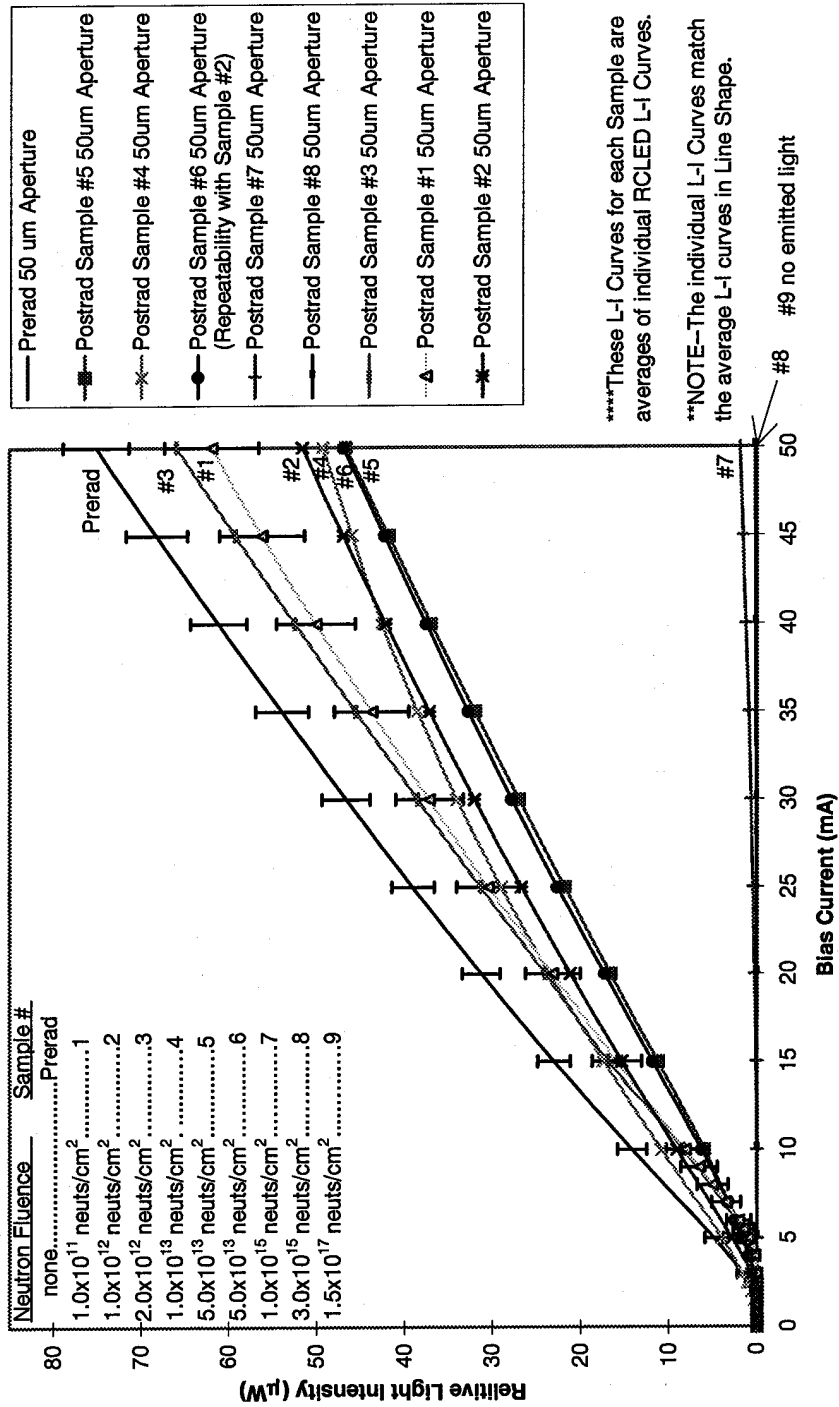Y-axis: Relitive Light Intensity (µW)

27

Figure 13. Measured emitted light power versus bias current for 50 µm apertures.
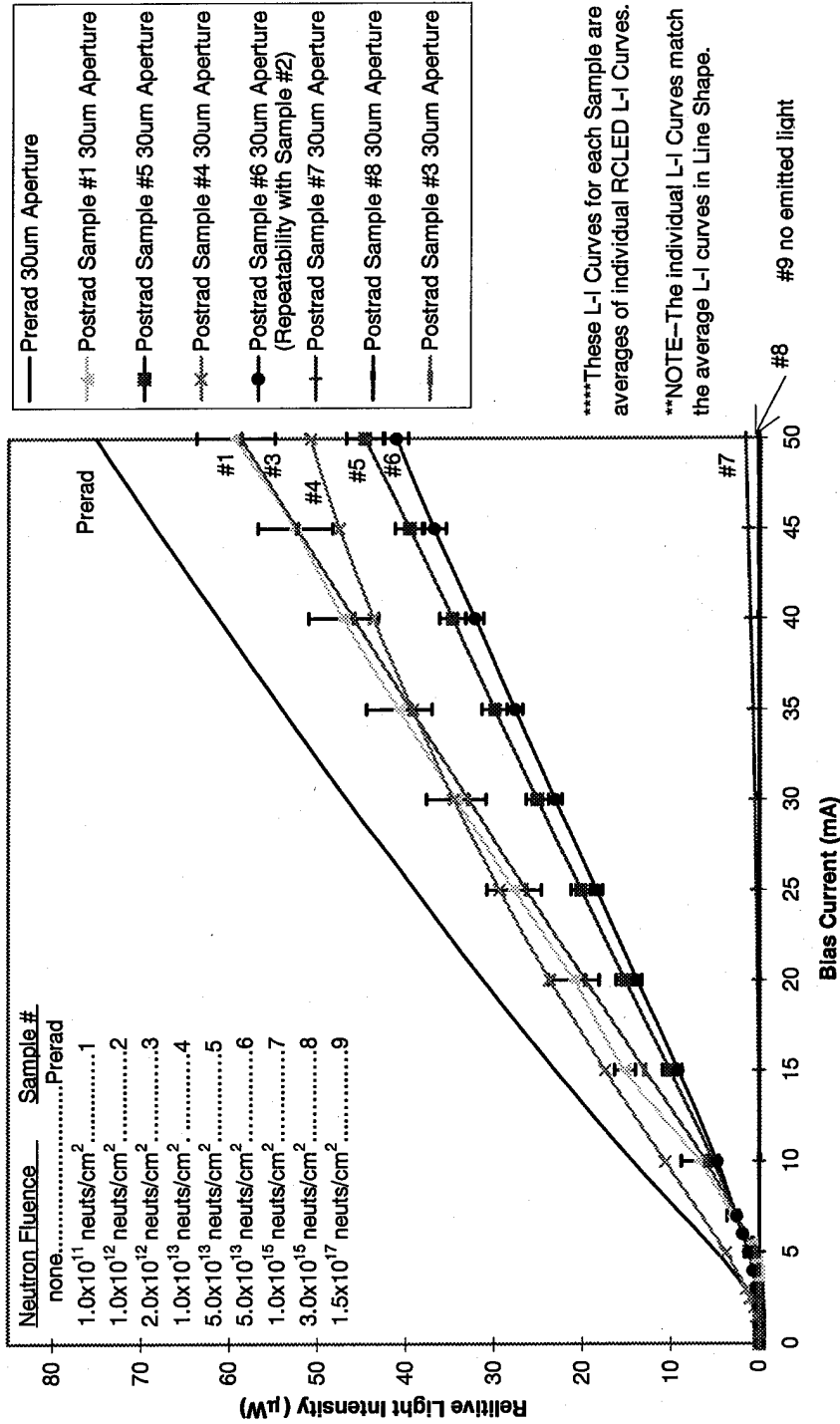
Theory has predicted the trends of degraded performance (curves #1 through #10) and repeatability (curves #5 and #6) shown in Figure 13. However, there are some discrepancies in Figure 13. The first discrepancy is the order of the L-I curves. The general trend of the L-I curves is a continual degrading of relative light power for each irradiation. The curves should be in order from no irradiation (Prerad) to the highest irradiation, where no light was generated at all. This is not the case for curve #1, #2, and #3. Curve #3 exposed to 2×10^{12} neutrons/cm^2 has a higher light output than curve #1, even though curve #1 was exposed to less of an irradiation (1×10^{11} neutrons/cm^2). Likewise, curves #2 was exposed to 1×10^{12} neutrons/cm^2 and should have a higher light output than curve #3 but it does not. This can be explained by experimental measurement error. The power meter used to obtain the data was very sensitive to position. It was not possible to place the power meter in exactly the same position each time for each measurement which is partially shown by the uncertainty bars on each of the L-I curves.

The other L-I curve, that looks different from the rest of the curves, is #4 (that was irradiated at 1×10^{13} neutrons/cm^2). The other curves are linear in nature whereas curve #4 is not linear, it is curved. The data for curve #4 was retaken and it confirmed its line shape. Curve #4 crosses curves #1, #2, and #3, suggesting that it has the same light intensity values as those curves for a given bias current. There are two possible explanations for this phenomenon. The first possibility is series resistance (see Figure 8). At high-injection levels there is an affect associated with the finite resistivity in the quasi-neutral regions of the junction [3]. This resistance absorbs a significant amount of the voltage drop across the diode. It has the effect that is shown in curve #4. The second possible reason for the effect shown in curve #4 is due to heating effects. When the

RCLED is injected with carriers, the device heats up. If the heating is too high, it has the effect of shifting the Fabry-Perot Dip (FPD-the pass band) and the Gain curve to longer wavelengths (red shifting). The gain curve shifts faster than the FPD does and at high temperatures only a small portion of gain curves sees the FPD. This has the effect shown in curve #4. Why the RCLEDs that produced curve #4 are the only devices out of all of the devices tested to have this effect, is undetermined at this time.

Similar results for the relative emitted light power of the RCLEDs, as a function of forward bias current at several different neutron fluences levels, are shown Figure 14. These plots are for a 30 μm aperture versus the 50 μm aperture above. There is again, a general trend of continued degradation in relative light power with each irradiation. There is also the same jump in degradation between curve #6 at 5×10^{13} neutrons/cm^2 and curve #7 at 3×10^{16} neutrons/cm^2 as was shown in Figure 13. Again, only some uncertainties are plotted. Finally, curve #4 shows the same effects as it did for a 50 μm aperture.

Figure 14. Measured emitted light power versus bias current for 30 μm apertures.

30

A second major area of interest is the relative light intensity versus neutron fluences (Φ) for a bias current of 50 mA with a 50 µm aperture, shown in Figure 15. A linear least squares fit was used to find a trend line equation (labeled on the chart). This shows there is definitely a logarithmic decrease in light intensity with increasing neutron fluence between 1×10^{12} neutrons/cm^2 and 5×10^{15} neutrons/cm^2. Note the R^2 value in regression analysis is a calculated value that indicates how valid a trend line is for forecasting. All of the R^2 values calculated are above 0.75 and the majority above 0.9 which indicates meaningful trend lines.

Also plotted and labeled in Figure 15 is the damage model equation. Mathcad 5.0 Plus was used to find the optimum damage constant K by minimizing the sum of the squares (the calculation method is given in Appendix A). At a bias current of 50 mA and a 50 µm aperture, the damage constant was calculated to be 4.9×10^{15} µW neutrons/cm^2.

Similar plots for a 50 µm aperture device are shown in Figure 16 for a 30 mA bias current and in Figure 17 for a 10 mA bias current.

Figure 15. Measured total emitted light power plotted versus fluence for a 50 μm aperture at a bias current of 50mA.

Relative Light Intensity Vs Neutron Fluence

Trend Line Equation
$y = -5.8972Ln(x) + 206.98$
$R^2 = 0.9617$

Damage Model Equation
$L_{tot}(\Phi) = (1/L_{toto} + \Phi/K)^{-1}$
Damage Constant
$K = 2.792 \times 10^{15}$ ($\mu W \times Neuts/cm^2$)

- ◆ Ltot @ I=30mA 50 um Aperture
- Least Squares Fit
- Log. (Ltot @ I=30mA 50 um Aperture)

Prerad Value

Neutron Fluence, Φ (Neuts/cm^2)

Relative Light Intensity (μW)

70 60 50 40 30 20 10 0

1.00E+10 1.00E+11 1.00E+12 1.00E+13 1.00E+14 1.00E+15 1.00E+16 1.00E+17
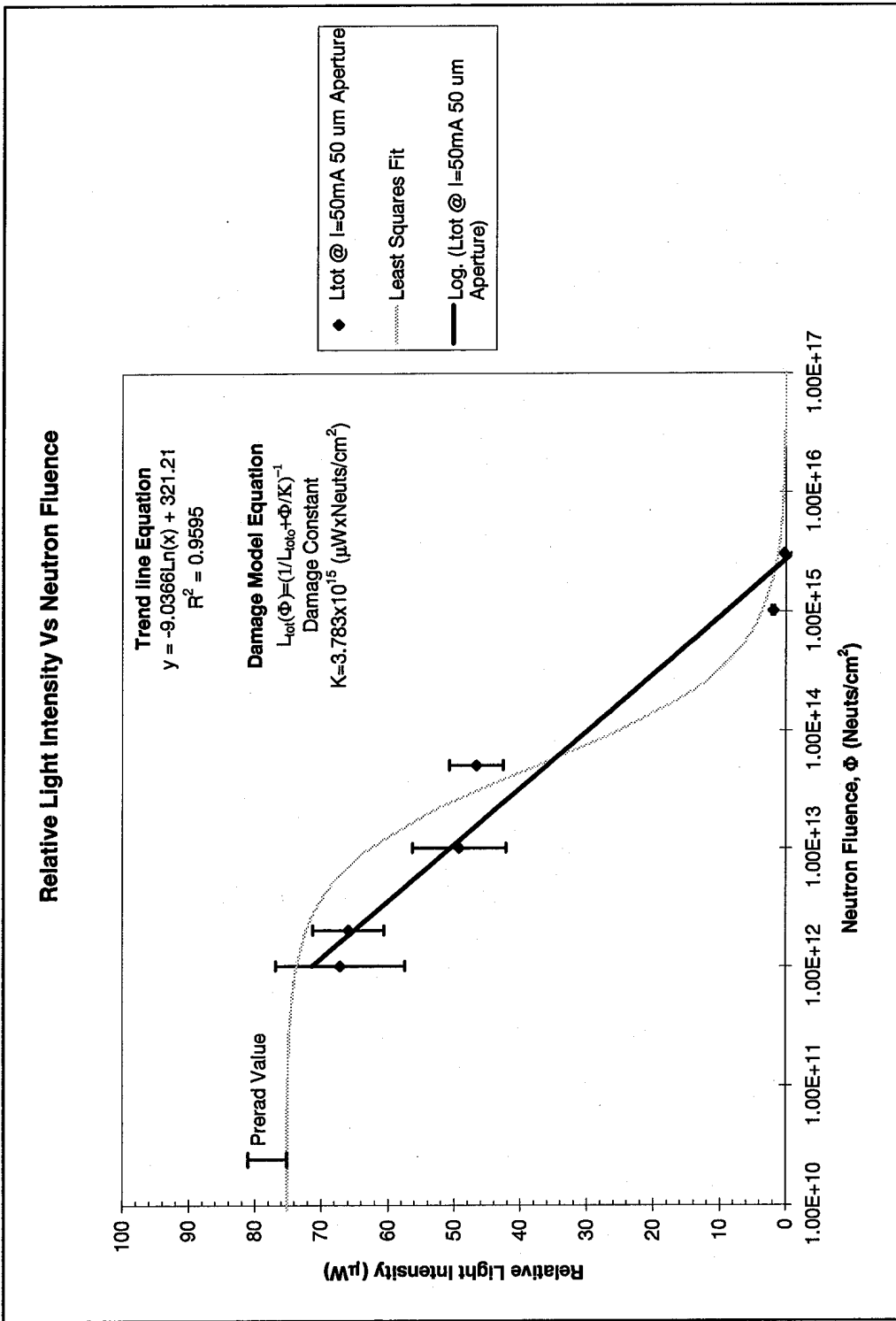
Figure 16. Measured total emitted light power plotted versus neutron fluence for a 50 μm aperture at a bias current of 30mA.

33

Figure 17. Measured total emitted light power plotted versus neutron fluence for a 50 μm aperture at a bias current of 10 mA.

These plots also show a logarithmic decrease in light intensity with increasing neutron fluence between 1×10^{12} neutrons/cm^2 and 5×10^{15} neutrons/cm^2. A damage constant K was calculated to be 2.8×10^{15} μW neutrons/cm^2 for 30 mA bias current and 4.9×10^{14} μW neutrons/cm^2 for 10 mA bias current. Similar plots are shown in Figure 18, Figure 19, and Figure 20 but these are for a 30 μm aperture versus 50 mA, 30 mA, and 10 mA bias current respectfully.

Figure 18. Measured total emitted light power plotted versus neutron fluence for a 30 μm aperture at a bias current of 50 mA
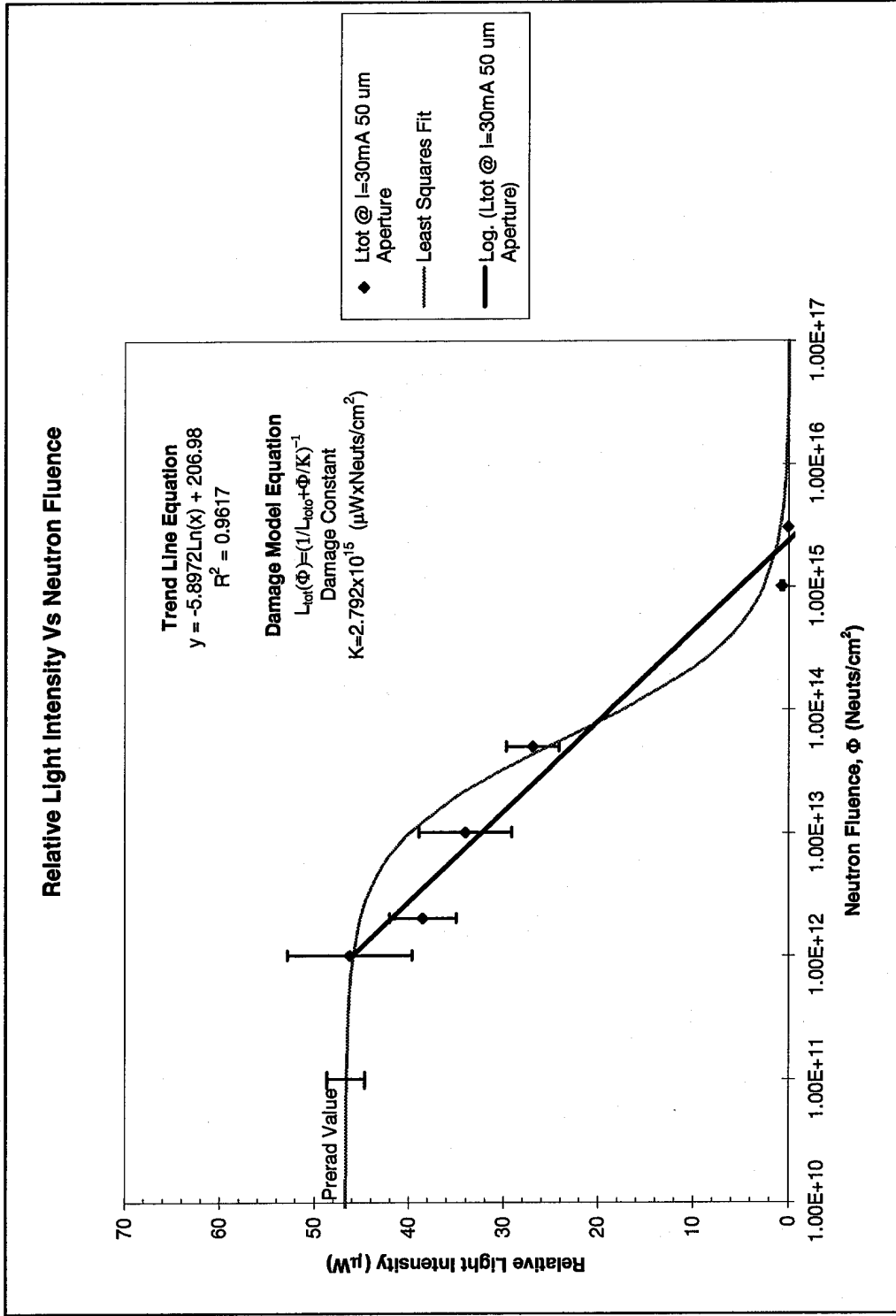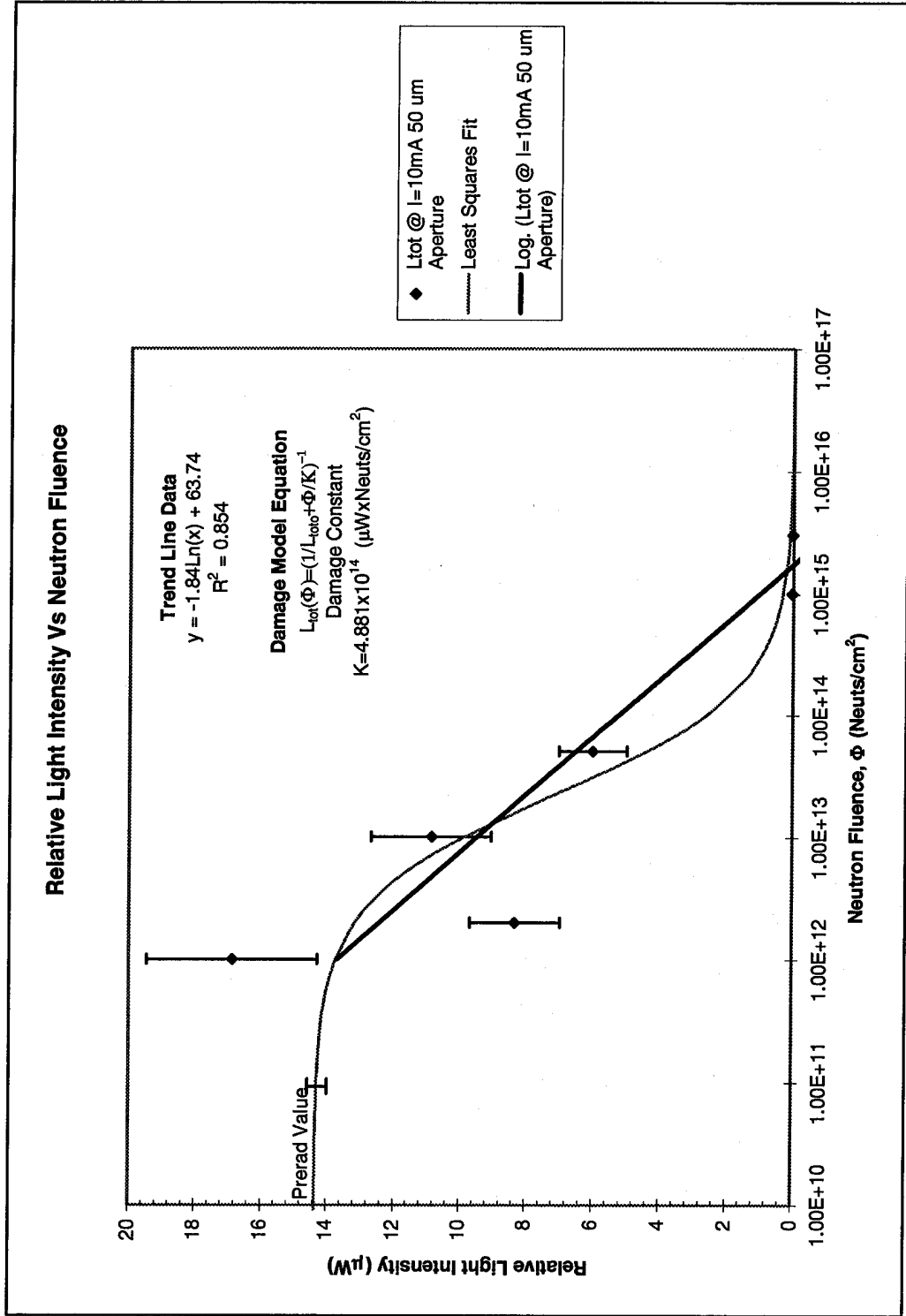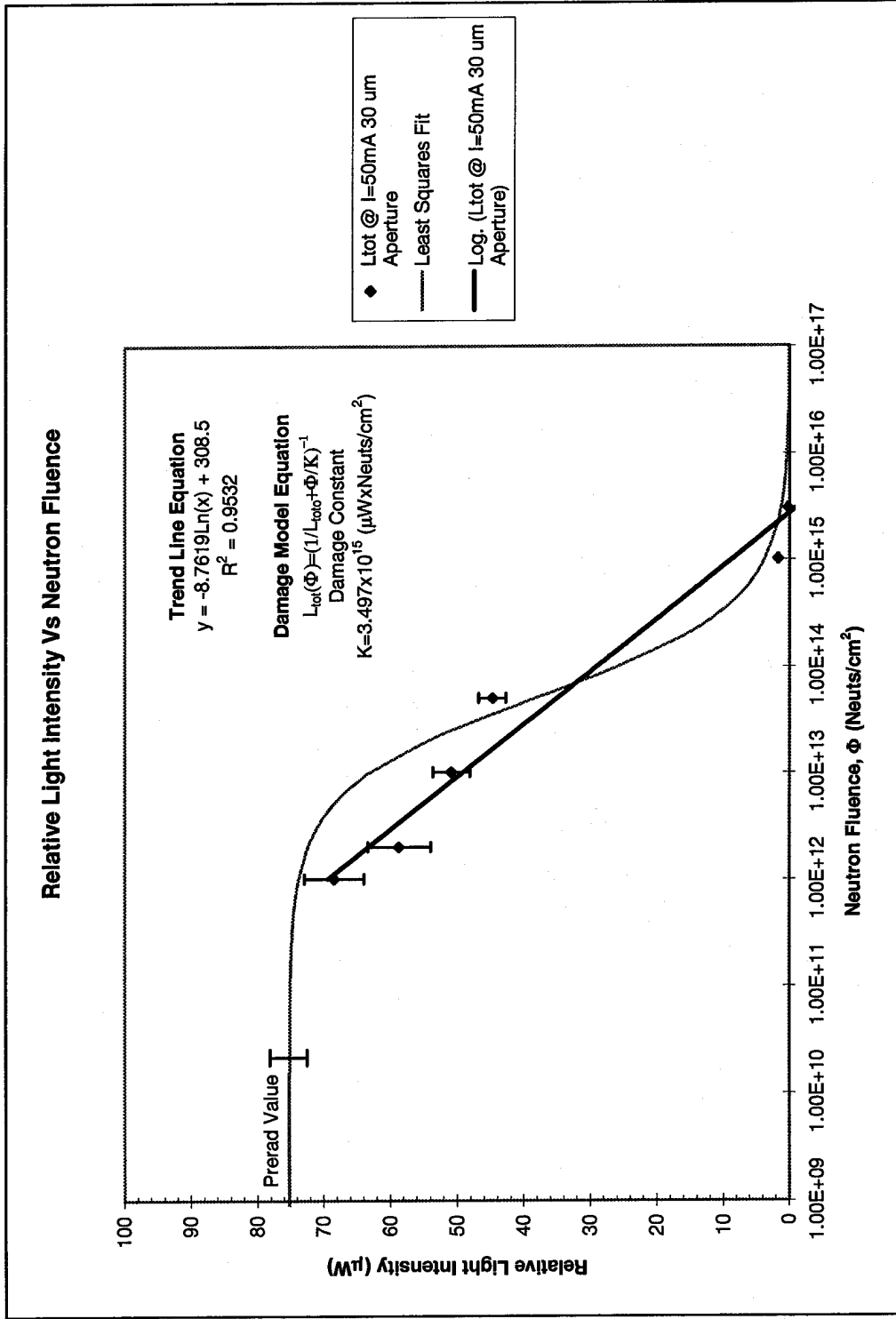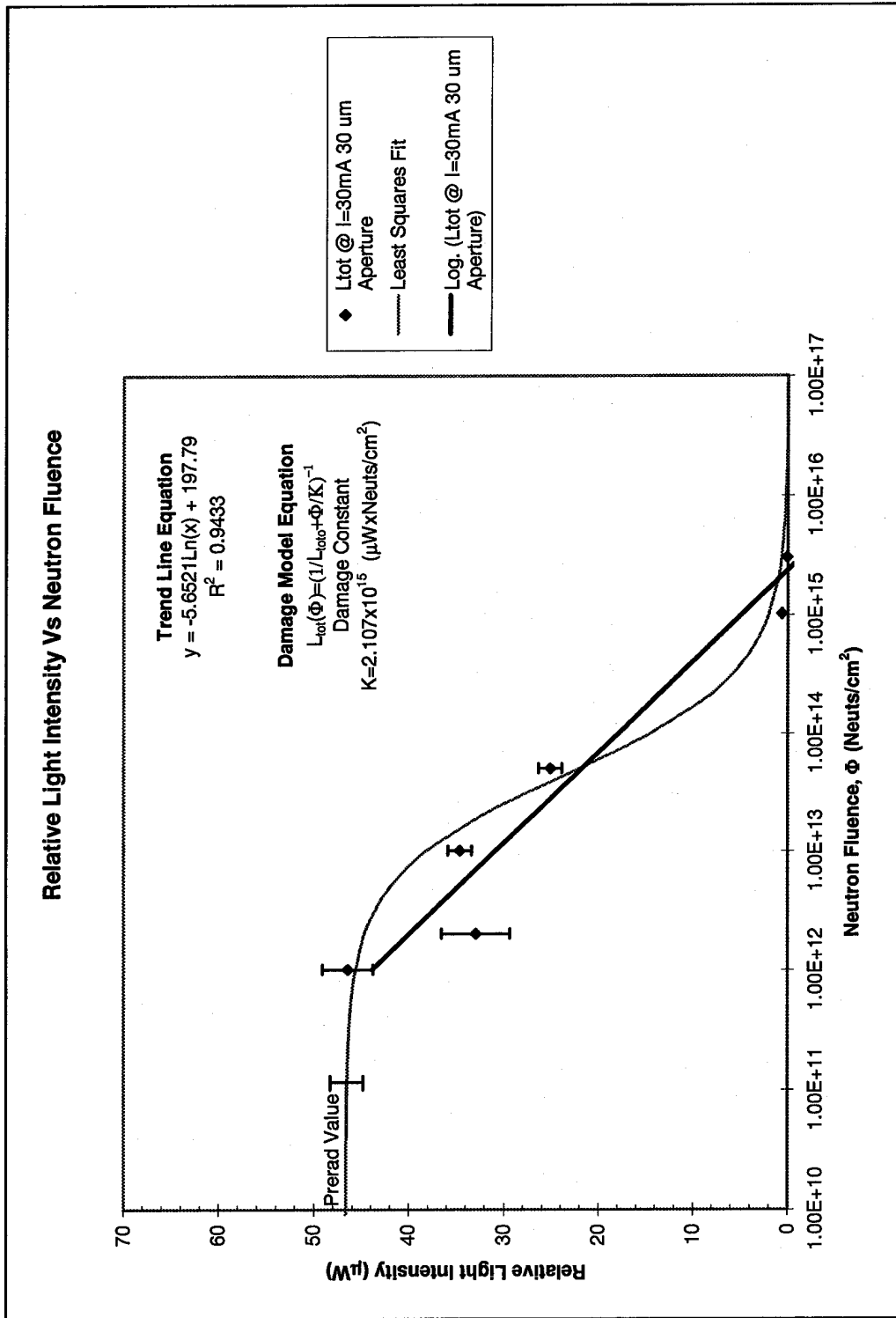
36

Figure 19. Measured total emitted light power plotted versus neutron fluence for a 30 μm Aperture at a bias current of 30mA.
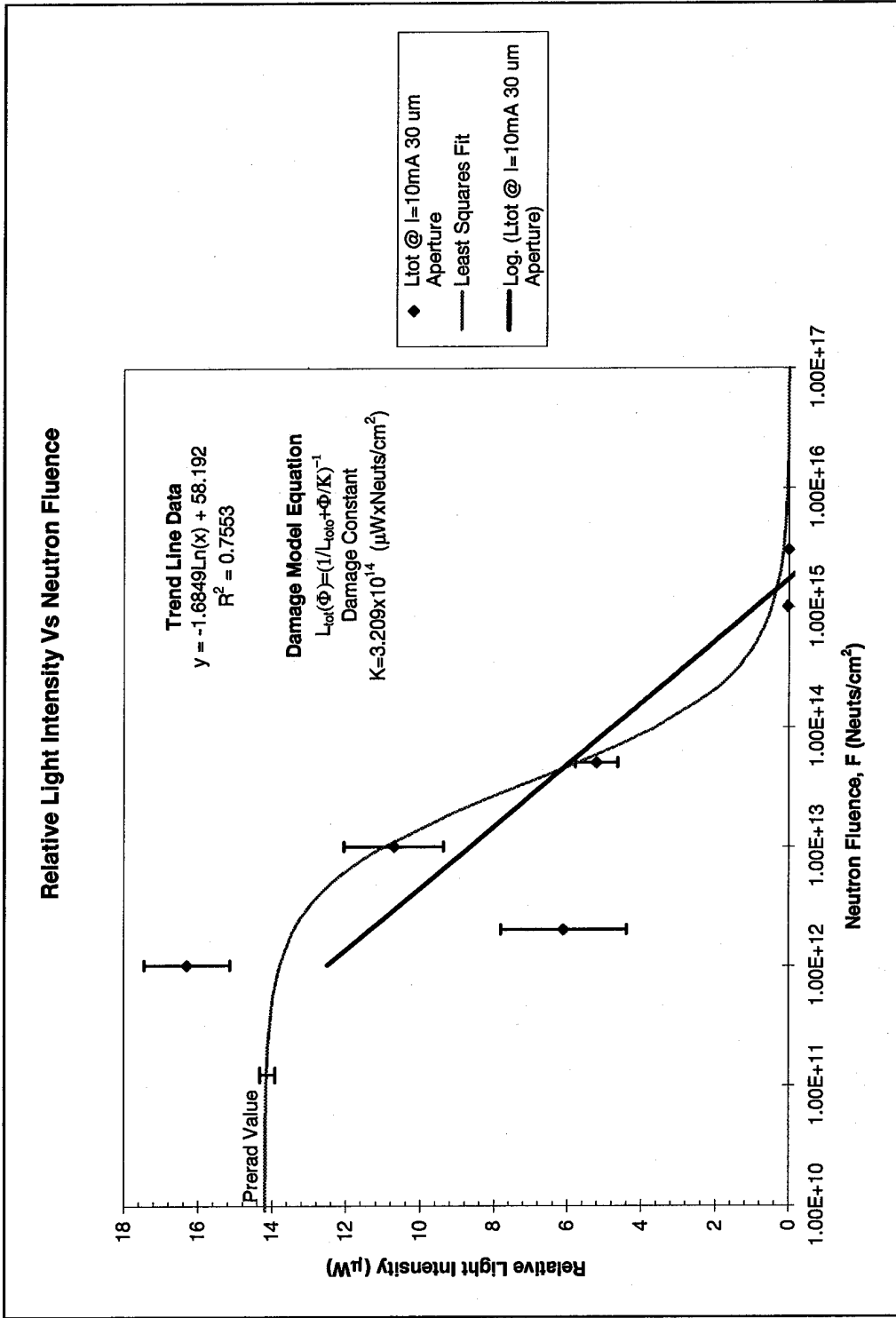
Figure 20. Measured total emitted light power plotted versus neutron fluence for a 30 μm Aperture at a bias current of 10mA.

Located in Table 4 are the calculated damage constant K values for the relative light intensity versus neutron fluence at a give bias current. There are two noticeable trends in the table. The first is, that as the bias current is decreased the damage constant decreases. The second is a decrease in the damage constant at a given bias current between a 50 μm aperture and a 30 μm aperture.

If K is decreasing, this means the damage model equation (labeled in the previous figures) is shifting to the left. With this shifting to the left, there is less relative light intensity at lower neutron fluences. The RCLED's performance is degrading for less of a neutron fluence. Also, as the K value is increased, the damage model equation is shifted to the right. A shifting to the right indicates higher relative light intensities at higher neutron fluences. This means a 30 μm aperture RCLED will not perform as well as a RCLED that has a 50 μm aperture, in a radiation filled-environment if these differences are significant. The 30 μm aperture appears more susceptible to damage.

Table 4. Summary of Damage Constants for Relative Light Intensity

Bias Current	50 μm Aperture	30 μm Aperture
50 mA	4.9×10^{15} μWneutrons/cm^2	3.5×10^{15} μWneutrons/cm^2
30 mA	2.8×10^{15} μWneutrons/cm^2	2.1×10^{15} μWneutrons/cm^2
10 mA	$4.9 10^{14}$ μWneutrons/cm^2	3.2×10^{14} μWneutrons/cm^2

The third parameter of interest is plotted in Figure 21 and is the differential quantum efficiency versus neutron fluences (Φ). A linear least squares fit was used to find a trend line equation (labeled on the chart). This shows there is definitely a

logarithmic decrease in differential quantum efficiency with neutron fluence between $1x10^{12}$ neutrons/cm^2 and $5x10^{15}$ neutrons/cm^2.

Also labeled on the chart is the damage model equation. Mathcad 5.0 Plus was again used to find the optimum damage constant K by minimizing the sum of the squares (located in Appendix A). For a 50 μm aperture, the damage constant was calculated to be $3.7x10^{13}$ neutrons/cm^2.

The degradation of the differential quantum efficiency is caused by traps in the bandgap [8]. These traps have the effect of reducing the minority carrier lifetimes which in-turn decrease the internal quantum efficiency resulting in a degraded differential quantum efficiency.

A similar plot is shown in Figure 22 but for a 30 μm aperture. The damage constant was calculated to be $4.7x10^{13}$ neutrons/cm^2.
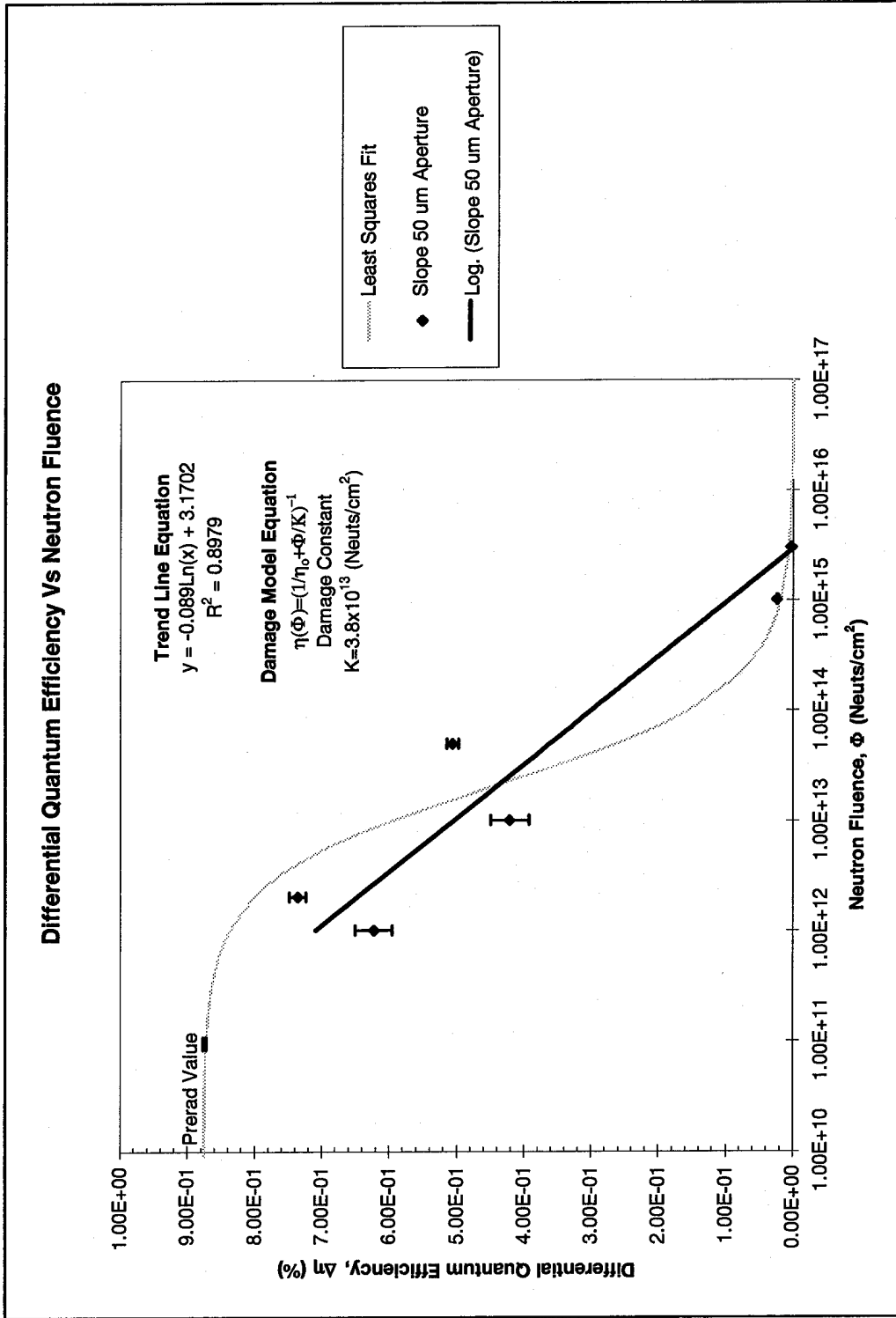
Figure 21. Differential quantum efficiency versus neutron fluence for a 50 µm aperture.
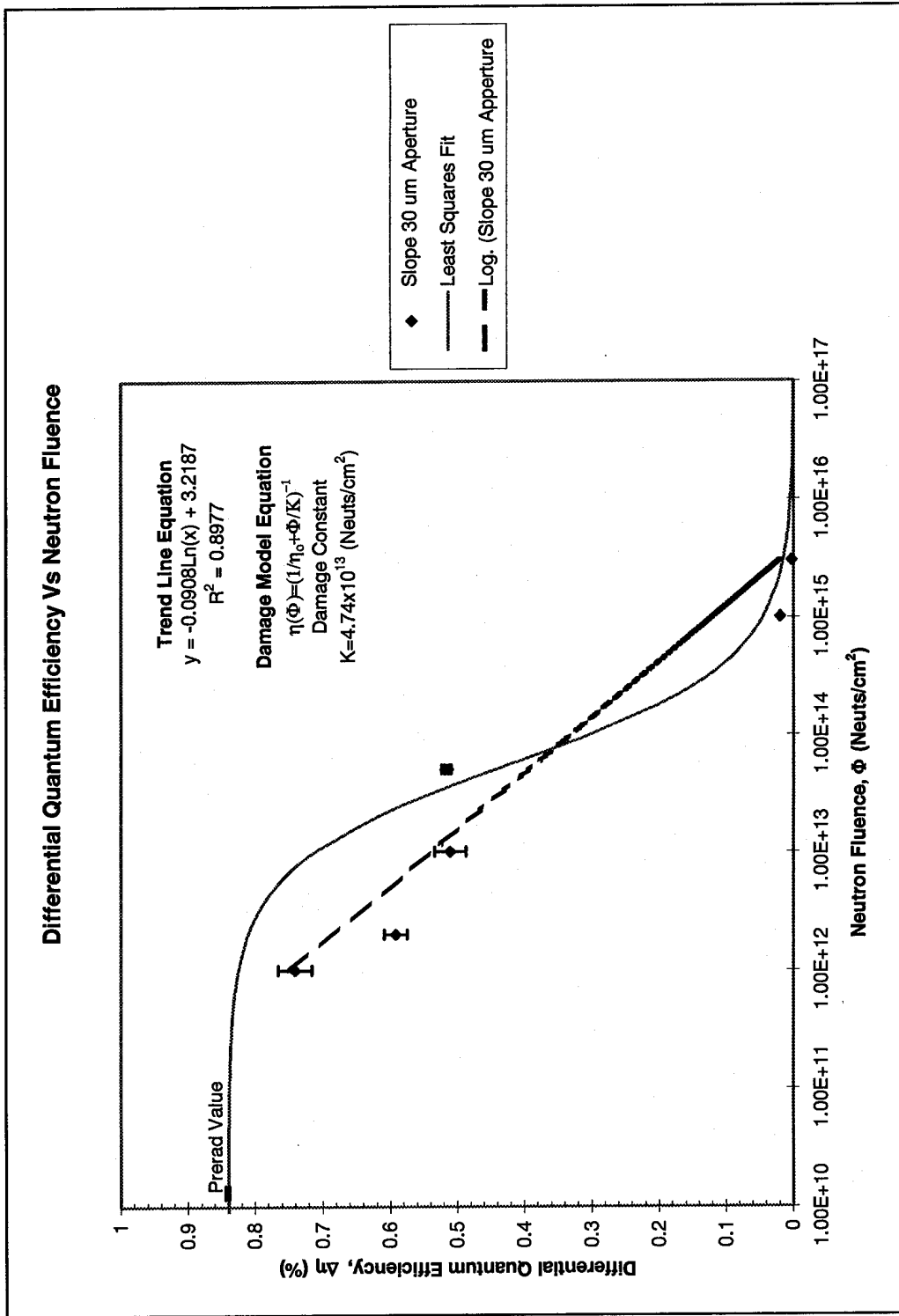
41

Figure 22. Differential quantum efficiency versus neutron fluence for a 30 μm aperture.

The fourth parameter of interest is the current versus voltage data. Like the relative light intensity and differential quantum efficiency, it was also collected for different neutron fluences with a 50 μm aperture. Located in Figure 23 is one example of an I-V curve at a healthy neutron fluence of 1.46×10^{17} neutrons/cm^2. There is an increase in the knee voltage of 0.14 volts indicating that the series resistance of the device has increased from the irradiation.

Current versus voltage data was also collected for different neutron fluences of a 30 μm aperture. Located in Figure 24 is an I-V curve for a 30 μm aperture that has been irradiated at 1.46×10^{17} neutrons/cm^2. There is an increase in the knee voltage of 0.18 volts.

The fifth parameter interest is the responsivity of the RCLED. The responsivity of the RCLED, with a 50 μm aperture, for varying amounts of neutron fluences is located in Figure 25. The general trend is that the responsivity of the RCLED decreases with increasing neutron fluence. The responsivity decreased for the same reason the differential quantum efficiency decreased; the minority carrier lifetime decreased.

Similar to the L-I curves, there are some non-ideal curves in Figure 25. The first discrepancy is the order of the curves. The general trend of the responsivity curves is a continual degrading of responsivity for each irradiation. The curves should be in order from no irradiation (Prerad) to the highest irradiation. This is not the case for curve #1 and #3. Curve #3 exposed to 2×10^{12} neutrons/cm^2 has a higher responsivity than curve #1, even though curve #1 was exposed to less of an irradiation (1×10^{11} neutrons/cm^2).

Figure 23. Bias Current Versus Measured Voltage for the RCLEDs of sample #1 with a 50 μm Aperture. This was the most heavily radiated sample. There is an increase in the knee voltage of 0.14 volts.
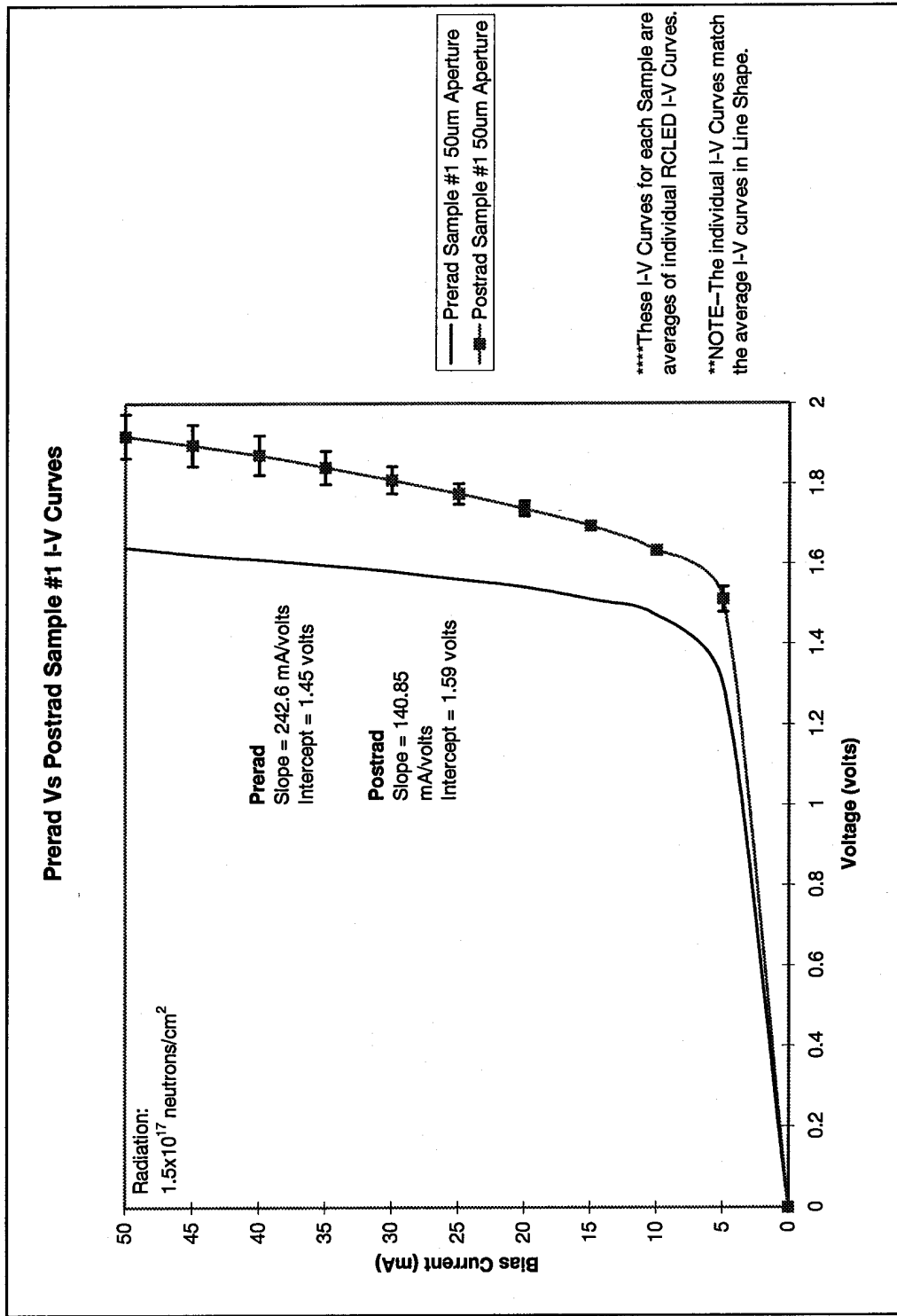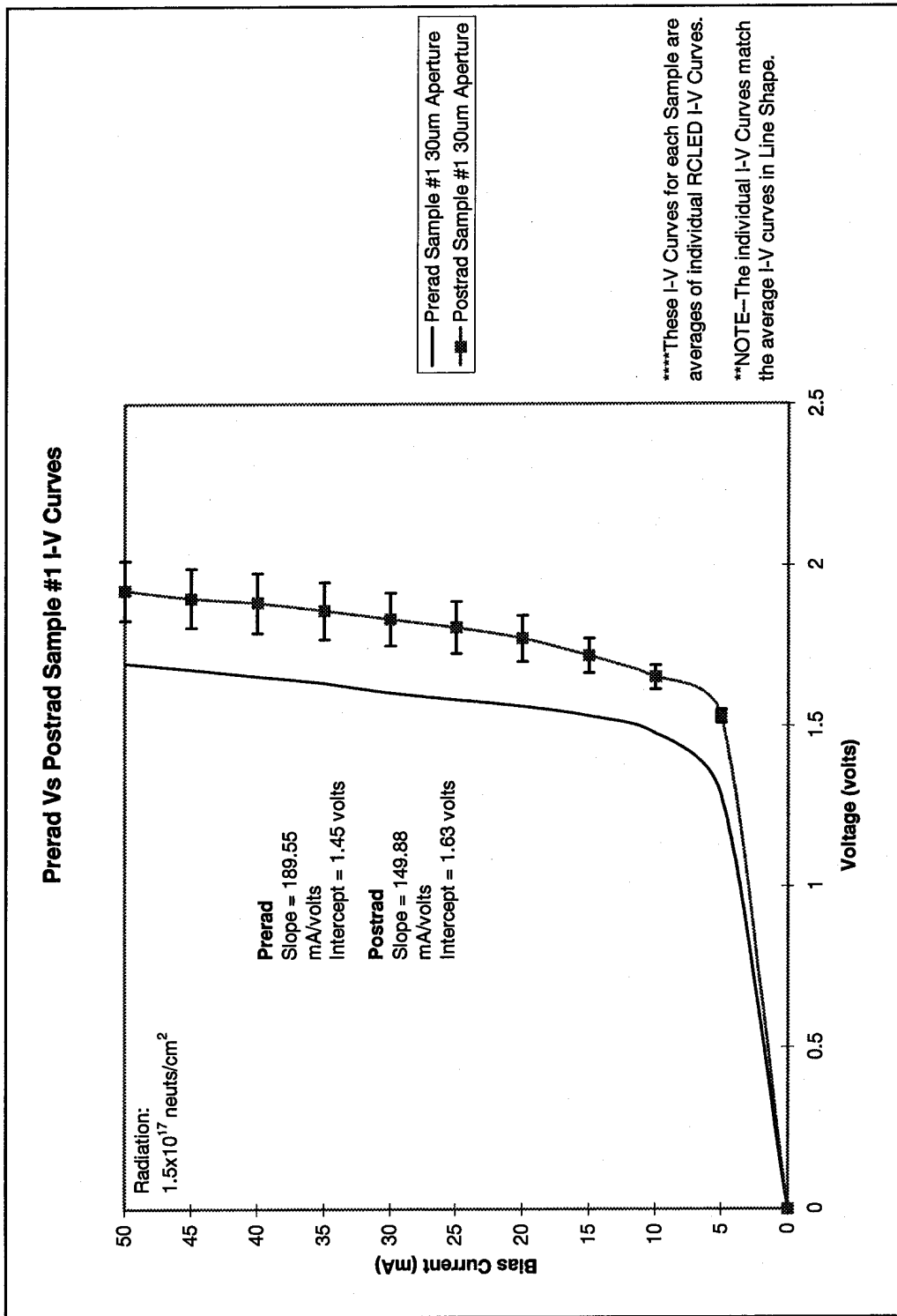
44

Figure 24. Bias Current Versus Measured Voltage for the RCLEDs of sample #1 with a 30 μm Aperture. This was the most heavily radiated sample. There is an increase in the knee voltage of 0.18 volts.
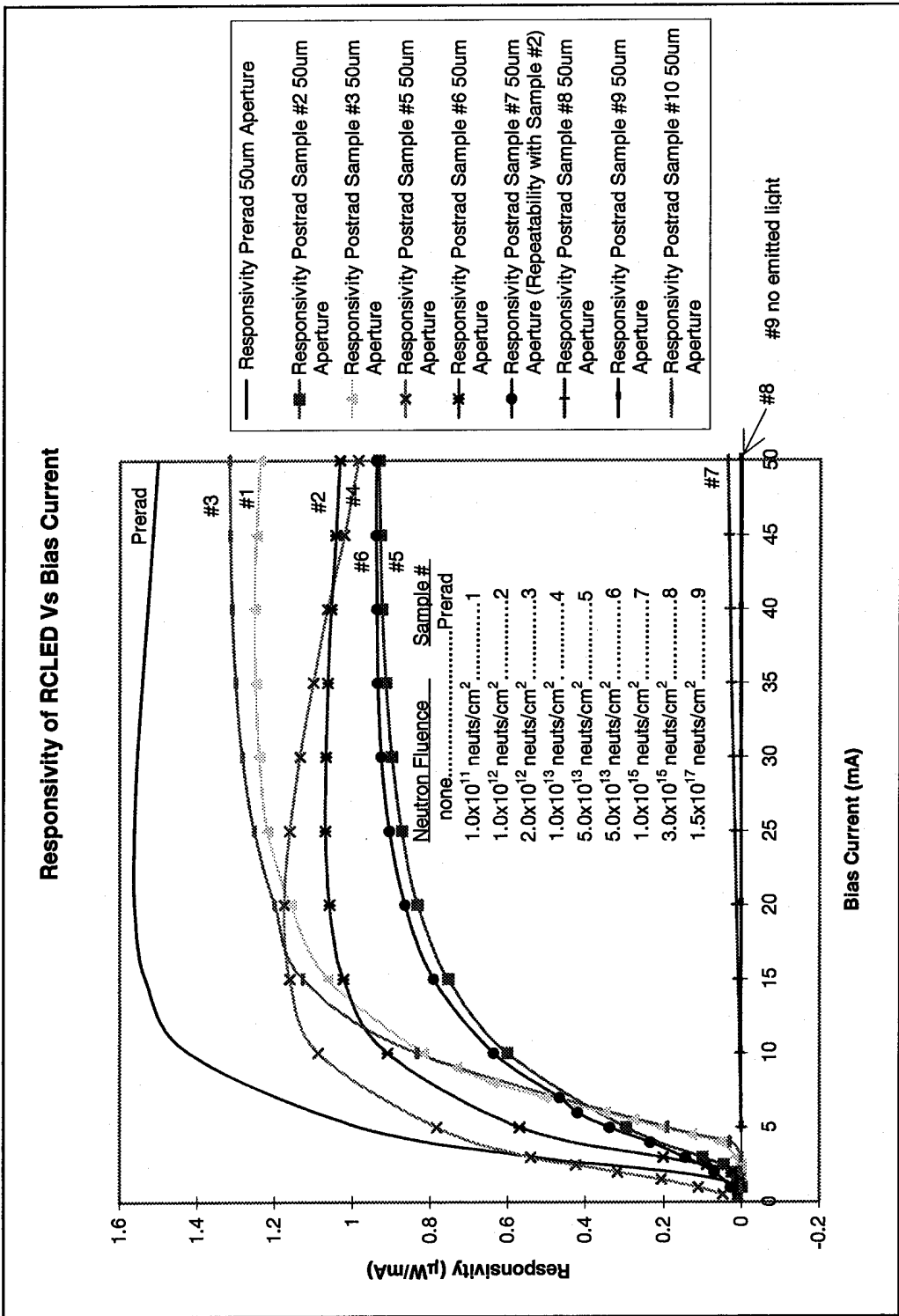
Figure 25. Responsivity of RCLED for varying neutron fluence.

The reason for this is tied directly into the L-I curves of Figure 13 and Figure 14 previously discussed. This is because the responsivity is nothing more than the emitted light power divided by the injected bias current. Also, Curve #4 shows the same effects of series resistance as it did in the L-I curves.

The sixth parameter of interest is the emitted spectral data. Spectral data was collected for the RCLED before and after irradiation. Located in Figure 26 is a typical emitted light spectrum from the RCLEDs. There is no significant change or trend in the peak wavelength or full-width-at-half maximum for any of the neutron fluences the RCLEDs saw. This means the Fabry-Perot Cavity, which determines the pass band of the emitted light, must not have been significantly altered or the FWHM would have showed more of a change. Therefore, the mirrors of the Fabry-Perot cavity do not seem to have changed in nature in any significant way due to the varying levels of neutron fluences.

Figure 26 lists the peak wavelengths and FWHMs for all the samples that were irradiated. This was for a 50 μm aperture and a 20 mA bias current. Similar results occurred for a 30 μm aperture.
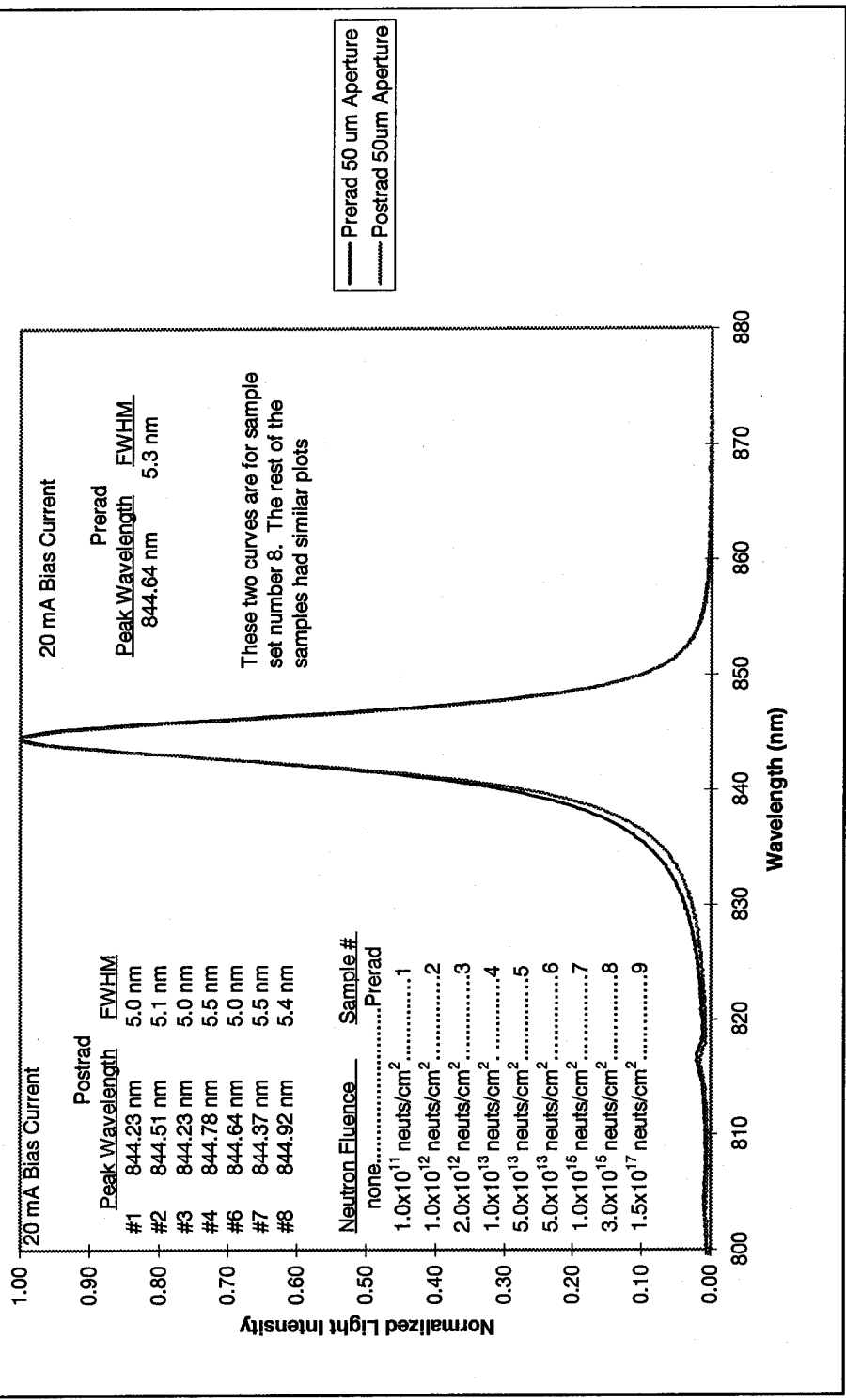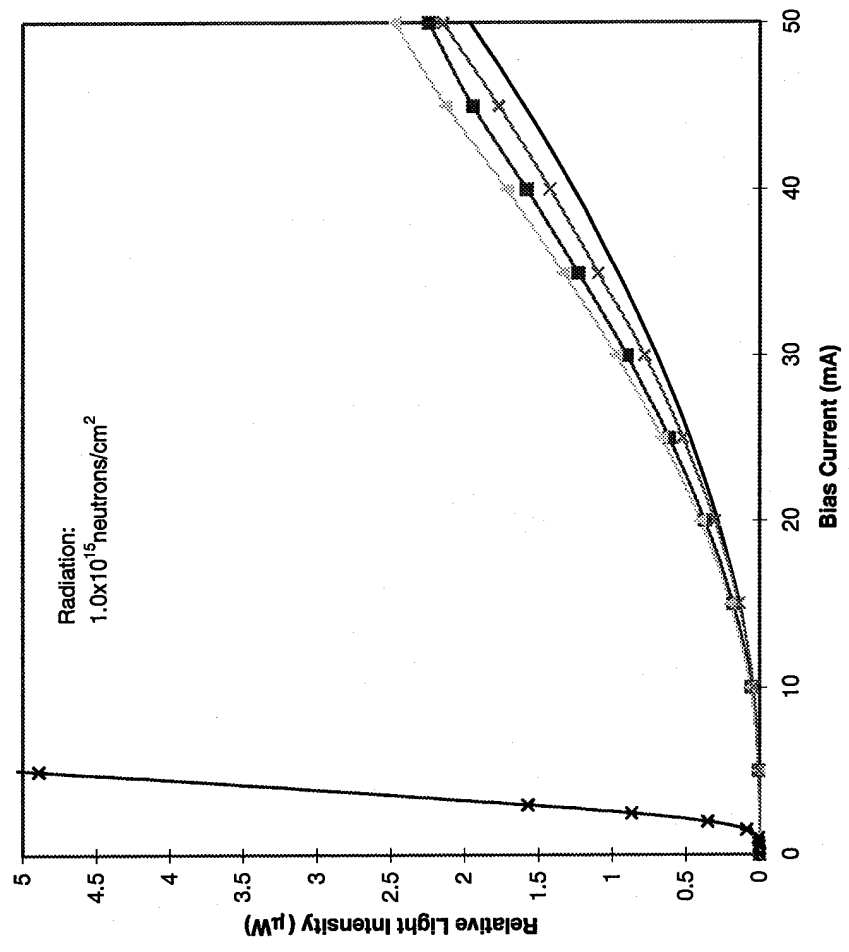
47

Figure 26. Spectrally inert to neutron irradiation.

The seventh and last parameter of interest is the annealing data. For annealing (and even for the previous measurements), it is important to know when the RCLEDs were irradiated and how long it was before they were characterized. Located in Table 3 of chapter III is a test matrix and dates of irradiation.

Located in Figure 27 is the L-I data after different levels of annealing for Sample #7. It shows that after six days of isothermal annealing (room temperature) there was an improvement in the relative light intensity versus bias current (six days was picked because no standard time period was located in the available ASTM). Improvement means an increased light intensity at a given bias current. The sample was then annealed isochronally (heated to 150° C for 10 min) and again there is improvement in the light intensity versus current (150° C for 10 min was selected because no standard time/temp was located in the available ASTM). Finally the sample was annealed again at 150° C for 10 min and this time the performance seemed to degrade. This would mean the device was already annealed and the device structure was changed because of excessive heat and/or time. However, a control sample was also characterized through all of the these annealing stages and did not show a degraded performance after the second 150° C for 10 min annealing. This means that the sensitive nature of the power meter (discussed in the L-I curves section), probably adversely effected the data of the second isochronal annealing.

Figure 28 shows another sample that was annealed in the same manner as above (Sample #8). It shows the same trend as above, improved performance. The same result after being heated for 150° C for 10 min. One key point to note is that the annealing at

Figure 27. Output light power versus two isochronal and one isothermal annealing.

50

Figure 28. Output light power versus one isochronal and isothermal annealing.

room temperature for Sample #7 was better than the room temperature annealing for Sample #8. This is because Sample #7 had sat around three days longer than Sample #8 giving it a chance to cure longer. Immediately after irradiation, damages begin to anneal out over time. After annealing for some time, a knee is reached, where the annealing effects begin to level out and eventually do level out (no more annealing takes place). The three days is believed to be on the knee of the annealing curve because neither Sample #7 or Sample #8 significantly annealed. Sample #7 is lower on the knee than Sample #8 which is why it annealed more than Sample #8. The effects of annealing were the final experimental data collected for this research project.

V Conclusion and Recommendations

Resonant Cavity Light-Emitting Diodes were irradiated to determine the effects of displacement damage. The RCLEDs were susceptible to neutron irradiation. Displacement damage, caused by the neutron irradiation [8], degraded the characteristics of the relative light intensity versus bias current for varying neutron fluence (Φ), total output light power versus Φ, differential quantum efficiency versus Φ, responsivity versus bias current for varying Φ, and bias current versus voltage curves for a specific Φ.

Logarithmic decreases in external light power and differential quantum efficiency with increasing neutron fluence were observed. Significant decreases in external light power were observed at neutron fluences greater than 5.1×10^{13} neutrons/cm^2. Therefore, the RCLEDs should not be used in applications that see higher fluences than this. If they were used, one could not expect any amount of performance from the device.

Equations were developed to predict the changes in external light power at a given bias current and the differential quantum efficiency for neutron fluences between 1×10^{10} neutrons/cm^2 to 1×10^{18} neutrons/cm^2. The damage constants for these equations were found from the irradiation data by minimizing the sum of squared residuals (example calculation in Appendix A) between the damage model and experimental data. The damage constants decreased for smaller aperture sizes and also decreased for smaller bias currents. This means a 30 µm aperture RCLED will not perform as well as a RCLED with a 50 µm aperture in a radiation filled environment.

The next parameter examined was the emitted spectral characteristic before and after irradiation. There were no significant changes in spectral distribution of the outputs

of the RCLEDs at neutron fluences up to 3×10^{15} neutrons/cm^2. Therefore, the mirrors of the Fabry-Perot cavity have not optically changed in any significant way due to the varying levels of neutron fluences.

After the neutron degradation of many of the RCLED properties were determined, the effects of annealing were investigated. Isothermal and isochronal annealing were performed with a marginal improvement of the RCLEDs output light power for a given bias current. After isochronal annealing one time at 150° C for 10 min, the extent of the RCLED's performance increase was fixed, i.e., the damages had annealed as far as they were going to.

Two recommendations are proposed for future work. A great improvement in collecting all the data could be accomplished by using a data acquisition board to collect the current, voltage, and light power readings. It would save one a lot of time and effort in collecting the data. It would also be a more consistent way of taking measurements because it is automated and the measurement setup remains a constant (it does not change which would affect the measurements) The second recommendation is to always have a control sample for all steps during data collection. This can save you days by not having to recheck data that does not make sense.

Bibliography

1 Craford, M.G. "LED's Challenge the Incandescents," *IEEE Circuits and Device Magazine*: 24-29 (September 1992).

2 Fitzgerald, Thomas M. *Design and Characterization of Resonant Cavity Light-Emitting Diodes*. MS thesis. AFIT/GEO/ENG/95D-02. School of Engineering, Air Force Institute of Technology (AU), Wright-Patterson AFB Oh, December 1994.

3 Sze, S. M. *Physics of Semiconductor Devices*. New York: Wiley-Interscience, 1981.

4 Hect, E. *Optics*, 2nd ed. Massachusetts: Addison Wesley Publishing Company, 1987.

5 Verdeyen, Joseph T. *Laser Electronics 2nd Edition*. New Jersey: Englewood Cliffs, 1995.

6 Gover, James E. *Basic Radiation Effects in Nuclear Power Electronics Technology*. New Mexico: California, 1986.

7 Messenger, George C. *The effects of Radiation on Electronic Systems*. New York: Van Nostrand Reinhold, 1992.

8 Walsh, Thomas E. *Effects of Neutron Radiation on Aluminum-Gallium-Arsenide Laser*. MS thesis. AFIT/GNE/PH/78-11.. School of Engineering, Air Force Institute of Technology (AU), Wright-Patterson AFB Oh, March 1978.

9 Summers, Geoffrey P. "Mechanism and Measurements," *IEEE Nuclear and Space Radiation Effects Conference Short Course*. NSREC, New Orleans: IV1-IV58 (1992).

10 Summers, Geoffrey P., Burke, E. A., and Dale, C. J. "Correlation of Particle-Induced Displacement Damage in Silicon," *IEEE Transactions on Nuclear Science*, Vol. NS-34, No. 6, (December 1987).

11 Summers, Geoffrey P. "Energy Dependence of Proton-Induced Displacement Damage in Gallium Arsenide," *IEEE Transactions on Nuclear Science*, Vol. NS-34, No. 6, (December 1987).

12   Luera, Theodore P. "Neutron Damage Equivalent for Silicon, Silicon Dioxide, and Gallium Arsenide," *IEEE Transactions on Nuclear Science,* Vol. NS-34, No. 6, (December 1987).

13   Barnes, D. E. "Neutron Damage in Epitaxial GaAs Laser Diodes," *Journal of Applied Physics*, Vol 30, No. 8, (August 1959).

14   Aukerman, L. W. "Radiation Effects in GaAs," *Journal of Applied Physics*, Vol 34, No. 12, (December 1963).

15   Kinchin, G. H. And Pease, R. S. *The Displacement of Atoms in Solids by Radiation.* Reports on Progress in Physics. Vol 18, 1955.

Appendix A Mathcad 5.0 Plus

Determination of the Damage Constant K

Differential Quantum Efficiency

or any other parameter versus Neutron Fluence

$$yy := \begin{bmatrix} 75.13333333 \\ 67.175 \\ 65.925 \\ 49.275 \\ 46.7 \\ 1.96 \\ 0.24475 \\ 0 \end{bmatrix}$$

Neutron Fluence

$$xx := \begin{bmatrix} 1.0 \cdot 10^0 \\ 1.01 \cdot 10^{12} \\ 2.02 \cdot 10^{12} \\ 1.01 \cdot 10^{13} \\ 5.06 \cdot 10^{13} \\ 1.01 \cdot 10^{15} \\ 3.03 \cdot 10^{15} \\ 1.46 \cdot 10^{17} \end{bmatrix}$$

Number of elements of xx

$$i := 0 .. \text{length}(xx) - 1$$

Data Points Plotted From Above

A-1
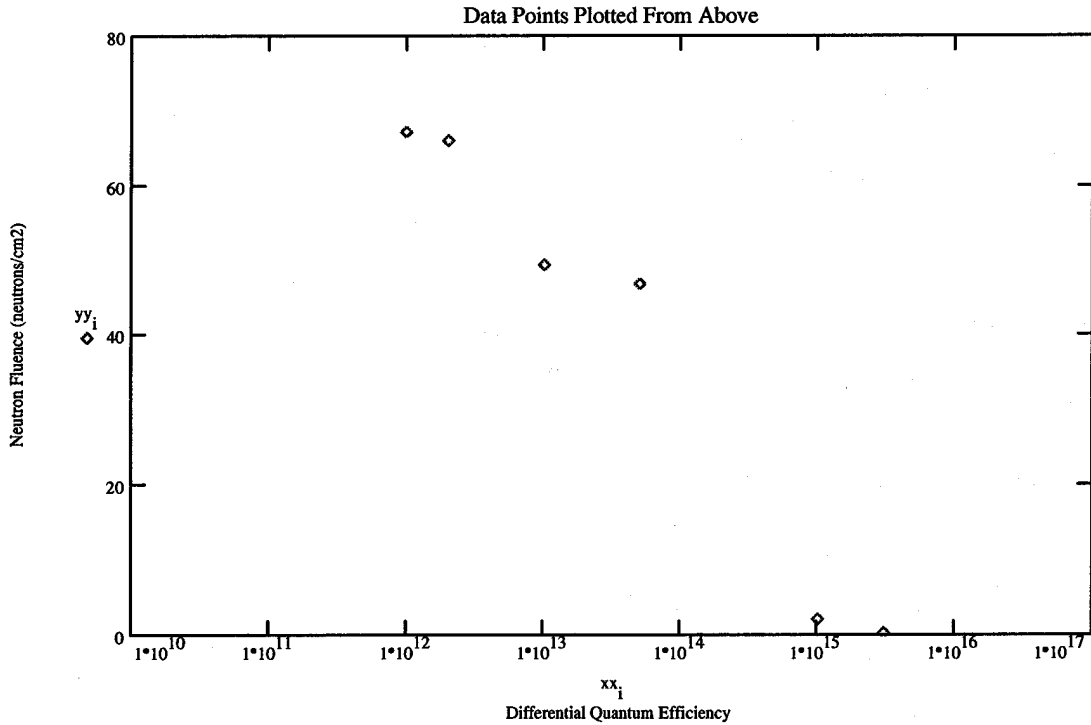
This is the equation that modles the Neutron Damage

$$F(x, K) := \left(\frac{1}{\eta_o} + \frac{x}{K} \right)^{-1}$$

Sum of Squares to be minimized

$$SSE(K) := \sum_i \left(yy_i - F(xx_i, K) \right)^2$$

$$\eta_o := yy_0$$
$$\eta_o = 75.133$$

Solve Block

Guess

$$K := 10^{15}$$

Given

$$SSE(K) = 0$$

$$Kfit := minerr(K)$$

$$Kfit = 3.786 \cdot 10^{15}$$

$$count := 50$$

$$g := 0 .. count$$

$$start := \log(10^8)$$

$$stop := \log(10^{19})$$

$$xxx_g := 10^{start + g \cdot \frac{stop - start}{count}}$$

Exponential form of Damage Model Equation

$$\eta_g := \eta_o \cdot e^{-\frac{xxx_g}{K}}$$

Damage Model Equation used to calculate K

$$\eta\eta_g := \frac{1}{\frac{1}{\eta_o} + \frac{xxx_g}{K}}$$

Log Regression of Best Fit

$$y_g := -.0883 \ln(xxx_g) + 3.1316$$

Differential Quantum Efficiency

yy_i ◇

$F(xxx_g, Kfit)$

η_g

$\eta\eta_g$

y_g

xx_i, xxx_g

Neutron Fluence (neutrons/cm2)
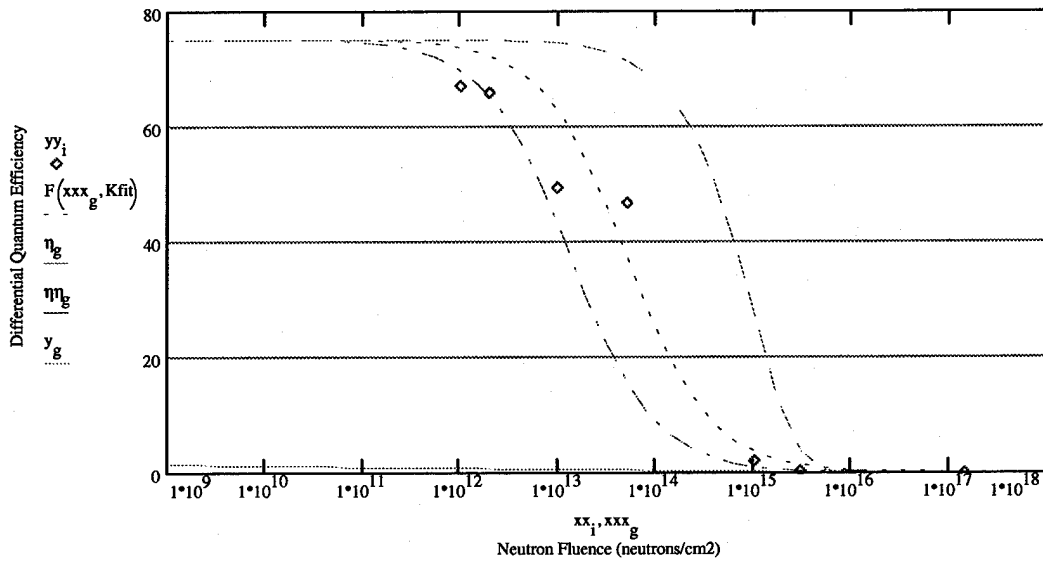
Vita

Second Lieutenant Daniel S. Hinkel ███████████████████

███████ He graduated from Greenwood High School in Millerstown, Pa (USA) in

1989 and attended Wilkes University Wilkes Barre, Pa, graduating in January 1994 with a

Bachelor of Science in Electrical Engineering. He began active duty in the U.S. Air

Force the same year, where he entered the School of Engineering, Air Force Institute of

Technology (AFIT), Wright-Patterson AFB, OH. In January 1996 he will be stationed at

Griffis AFB, NY, working in ROME Lab's Photonics Division.

REPORT DOCUMENTATION PAGE

Public reporting burden for this collection of information is estimated to average 1 hour per response, including the time for reviewing instructions, searching existing data sources, gathering and maintaining the data needed, and completing and reviewing the collection of information. Send comments regarding this burden estimate or any other aspect of this collection of information, including suggestions for reducing this burden. to Washington Headquarters Services, Directorate for Information Operations and Reports, 1215 Jefferson Davis Highway, Suite 1204, Arlington, VA 22202-4302, and to the Office of Management and Budget, Paperwork Reduction Project (0704-0188), Washington, DC 20503.

1. AGENCY USE ONLY (Leave blank)	2. REPORT DATE December 1995	3. REPORT TYPE AND DATES COVERED Master's Thesis

4. TITLE AND SUBTITLE
Effects of Neutron Radiation on Resonant Cavity Light-Emitting Diodes

5. FUNDING NUMBERS

6. AUTHOR(S)
Daniel S. Hinkel
2nd Lt, USAF

7. PERFORMING ORGANIZATION NAME(S) AND ADDRESS(ES)

Air Force Institute of Technology, WPAFB OH 45433-6568

8. PERFORMING ORGANIZATION REPORT NUMBER

AFIT/GEO/ENP/95D-01

9. SPONSORING / MONITORING AGENCY NAME(S) AND ADDRESS(ES)

Capt Charles P. Brothers, Jr
PL/VTET
3550 Aberdeen Avenue S.E.
Kirtland AFB NM 87117-5776

10. SPONSORING / MONITORING AGENCY REPORT NUMBER

11. SUPPLEMENTARY NOTES

12a. DISTRIBUTION / AVAILABILITY STATEMENT

Approved for public release; Distribution Unlimited

12b. DISTRIBUTION CODE

13. ABSTRACT (Maximum 200 words)

Resonant Cavity Light-Emitting Diodes (RCLEDs) were irradiated in Ohio State University's nuclear reactor to determine the effects of Neutron displacement damage. The RCLEDs were characterized both before and after irradiation by their current versus voltage curves (I-V curves) and external light power versus current curves (L-I curves). The I-V curves showed an increase in the "knee voltage" at a neutron fluence of 1.45×10^{17} neutrons/cm^2. Logarithmic decreases in external light power and differential quantum efficiency were observed. Significant decreases in external light power were observed at neutron fluences greater than 5.1×10^{13} neutrons/cm^2. Equations were developed to predict the changes in external light power at a given bias current and the differential quantum efficiency for neutron fluences between 1×10^{10} neutrons/cm^2 to 1×10^{18} neutrons/cm^2. The damage constants for these equations were derived from the irradiation data. Finally, there was no significant changes in the RCLED output spectral distribution at neutron fluences up to 3×10^{15} neutrons/cm^2.

14. SUBJECT TERMS
Diodes RCLED LED Neutron Radiation Resonant Cavity Quantum Well

15. NUMBER OF PAGES
69

16. PRICE CODE

17. SECURITY CLASSIFICATION OF REPORT	18. SECURITY CLASSIFICATION OF THIS PAGE	19. SECURITY CLASSIFICATION OF ABSTRACT	20. LIMITATION OF ABSTRACT
UNCLASSIFIED	UNCLASSIFIED	UNCLASSIFIED	UL

GENERAL INSTRUCTIONS FOR COMPLETING SF 298

The Report Documentation Page (RDP) is used in announcing and cataloging reports. It is important that this information be consistent with the rest of the report, particularly the cover and title page. Instructions for filling in each block of the form follow. It is important to *stay within the lines* to meet *optical scanning requirements*.

Block 1. Agency Use Only *(Leave blank)*.

Block 2. Report Date. Full publication date including day, month, and year, if available (e.g. 1 Jan 88). Must cite at least the year.

Block 3. Type of Report and Dates Covered. State whether report is interim, final, etc. If applicable, enter inclusive report dates (e.g. 10 Jun 87 - 30 Jun 88).

Block 4. Title and Subtitle. A title is taken from the part of the report that provides the most meaningful and complete information. When a report is prepared in more than one volume, repeat the primary title, add volume number, and include subtitle for the specific volume. On classified documents enter the title classification in parentheses.

Block 5. Funding Numbers. To include contract and grant numbers; may include program element number(s), project number(s), task number(s), and work unit number(s). Use the following labels:

C	-	Contract	**PR** -	Project
G	-	Grant	**TA** -	Task
PE	-	Program Element	**WU** -	Work Unit Accession No.

Block 6. Author(s). Name(s) of person(s) responsible for writing the report, performing the research, or credited with the content of the report. If editor or compiler, this should follow the name(s).

Block 7. Performing Organization Name(s) and Address(es). Self-explanatory.

Block 8. Performing Organization Report Number. Enter the unique alphanumeric report number(s) assigned by the organization performing the report.

Block 9. Sponsoring/Monitoring Agency Name(s) and Address(es). Self-explanatory.

Block 10. Sponsoring/Monitoring Agency Report Number. *(If known)*

Block 11. Supplementary Notes. Enter information not included elsewhere such as: Prepared in cooperation with...; Trans. of...; To be published in.... When a report is revised, include a statement whether the new report supersedes or supplements the older report.

Block 12a. Distribution/Availability Statement. Denotes public availability or limitations. Cite any availability to the public. Enter additional limitations or special markings in all capitals (e.g. NOFORN, REL, ITAR).

DOD	-	See DoDD 5230.24, "Distribution Statements on Technical Documents."
DOE	-	See authorities.
NASA	-	See Handbook NHB 2200.2.
NTIS	-	Leave blank.

Block 12b. Distribution Code.

DOD	-	Leave blank.
DOE	-	Enter DOE distribution categories from the Standard Distribution for Unclassified Scientific and Technical Reports.
NASA	-	Leave blank.
NTIS	-	Leave blank.

Block 13. Abstract. Include a brief *(Maximum 200 words)* factual summary of the most significant information contained in the report.

Block 14. Subject Terms. Keywords or phrases identifying major subjects in the report.

Block 15. Number of Pages. Enter the total number of pages.

Block 16. Price Code. Enter appropriate price code *(NTIS only)*.

Blocks 17. - 19. Security Classifications. Self-explanatory. Enter U.S. Security Classification in accordance with U.S. Security Regulations (i.e., UNCLASSIFIED). If form contains classified information, stamp classification on the top and bottom of the page.

Block 20. Limitation of Abstract. This block must be completed to assign a limitation to the abstract. Enter either UL (unlimited) or SAR (same as report). An entry in this block is necessary if the abstract is to be limited. If blank, the abstract is assumed to be unlimited.